



# TECH BRIEFS

NATIONAL AERONAUTICS AND SPACE ADMINISTRATION

-  **Technology Focus**
-  **Electronics/Computers**
-  **Software**
-  **Materials**
-  **Mechanics/Machinery**
-  **Manufacturing**
-  **Bio-Medical**
-  **Physical Sciences**
-  **Information Sciences**
-  **Books and Reports**



## INTRODUCTION

Tech Briefs are short announcements of innovations originating from research and development activities of the National Aeronautics and Space Administration. They emphasize information considered likely to be transferable across industrial, regional, or disciplinary lines and are issued to encourage commercial application.

### Availability of NASA Tech Briefs and TSPs

Requests for individual Tech Briefs or for Technical Support Packages (TSPs) announced herein should be addressed to

#### National Technology Transfer Center

Telephone No. (800) 678-6882 or via World Wide Web at [www.nttc.edu](http://www.nttc.edu)

Please reference the control numbers appearing at the end of each Tech Brief. Information on NASA's Innovative Partnerships Program (IPP), its documents, and services is also available at the same facility or on the World Wide Web at <http://www.nasa.gov/offices/ipp/network/index.html>

Innovative Partnerships Offices are located at NASA field centers to provide technology-transfer access to industrial users. Inquiries can be made by contacting NASA field centers listed below.

## NASA Field Centers and Program Offices

#### Ames Research Center

Lisa L. Lockyer  
(650) 604-1754  
[lisa.l.lockyer@nasa.gov](mailto:lisa.l.lockyer@nasa.gov)

#### Dryden Flight Research Center

Gregory Poteat  
(661) 276-3872  
[greg.poteat@dfrc.nasa.gov](mailto:greg.poteat@dfrc.nasa.gov)

#### Glenn Research Center

Kathy Needham  
(216) 433-2802  
[kathleen.k.needham@nasa.gov](mailto:kathleen.k.needham@nasa.gov)

#### Goddard Space Flight Center

Nona Checks  
(301) 286-5810  
[nona.k.checks@nasa.gov](mailto:nona.k.checks@nasa.gov)

#### Jet Propulsion Laboratory

Andrew Gray  
(818) 354-3821  
[gray@jpl.nasa.gov](mailto:gray@jpl.nasa.gov)

#### Johnson Space Center

information  
(281) 483-3809  
[jsc.techtran@mail.nasa.gov](mailto:jsc.techtran@mail.nasa.gov)

#### Kennedy Space Center

David R. Makufka  
(321) 867-6227  
[david.r.makufka@nasa.gov](mailto:david.r.makufka@nasa.gov)

#### Langley Research Center

Brian Beaton  
(757) 864-2192  
[brian.f.beaton@nasa.gov](mailto:brian.f.beaton@nasa.gov)

#### Marshall Space Flight Center

Jim Dowdy  
(256) 544-7604  
[jim.dowdy@msfc.nasa.gov](mailto:jim.dowdy@msfc.nasa.gov)

#### Stennis Space Center

Ramona Travis  
(228) 688-3832  
[ramona.e.travis@nasa.gov](mailto:ramona.e.travis@nasa.gov)

#### Carl Ray, Program Executive

Small Business Innovation  
Research (SBIR) & Small  
Business Technology  
Transfer (STTR) Programs  
(202) 358-4652  
[carl.g.ray@nasa.gov](mailto:carl.g.ray@nasa.gov)

#### Doug Comstock, Director

Innovative Partnerships  
Program Office  
(202) 358-2560  
[doug.comstock@nasa.gov](mailto:doug.comstock@nasa.gov)





# TECH BRIEFS

NATIONAL AERONAUTICS AND SPACE ADMINISTRATION



## 5 Technology Focus: Sensors

- 5 Light-Driven Polymeric Bimorph Actuators
- 6 Guaranteeing Failsafe Operation of Extended-Scene Shack-Hartmann Wavefront Sensor Algorithm
- 6 Cloud Water Content Sensor for Sounding Balloons and Small UAVs
- 6 Pixelized Device Control Actuators for Large Adaptive Optics
- 7 T-Slide Linear Actuators



## 9 Electronics/Computers

- 9 G<sup>4</sup>FET Implementations of Some Logic Circuits
- 10 Electrically Variable or Programmable Nonvolatile Capacitors
- 11 System for Automated Calibration of Vector Modulators
- 12 Complementary Paired G<sup>4</sup>FETs as Voltage-Controlled NDR Device
- 13 Three MMIC Amplifiers for the 120-to-200 GHz Frequency Band
- 14 Low-Noise MMIC Amplifiers for 120 to 180 GHz



## 15 Materials

- 15 Using Ozone To Clean and Passivate Oxygen-Handling Hardware
- 15 Metal Standards for Waveguide Characterization of Materials
- 16 Two-Piece Screens for Decontaminating Granular Material



## 17 Manufacturing & Prototyping

- 17 Mercuric Iodide Anticoincidence Shield for Gamma-Ray Spectrometer
- 17 Improved Method of Design for Folding Inflatable Shells



## 19 Mechanics/Machinery

- 19 Ultra-Large Solar Sail
- 19 Cooperative Three-Robot System for Traversing Steep Slopes
- 20 Assemblies of Conformal Tanks
- 21 Microfluidic Pumps Containing Teflon<sup>®</sup> AF Diaphragms



## 23 Physical Sciences

- 23 Transparent Conveyor of Dielectric Liquids or Particles
- 24 Multi-Cone Model for Estimating GPS Ionospheric Delays
- 25 High-Sensitivity GaN Microchemical Sensors
- 26 On the Divergence of the Velocity Vector in Real-Gas Flow
- 26 Progress Toward a Compact, Highly Stable Ion Clock
- 27 Instruments for Imaging From Far to Near
- 28 Reflectors Made From Membranes Stretched Between Beams



## 29 Information Sciences

- 29 Integrated Risk and Knowledge Management Program — IRKM-P
- 30 LDPC Codes With Minimum Distance Proportional to Block Size
- 31 Constructing LDPC Codes From Loop-Free Encoding Modules



## 33 Books & Reports

- 33 MMICs With Radial Probe Transitions to Waveguides
- 33 Tests of Low-Noise MMIC Amplifier Module at 290 to 340 GHz
- 33 Extending Newtonian Dynamics to Include Stochastic Processes

This document was prepared under the sponsorship of the National Aeronautics and Space Administration. Neither the United States Government nor any person acting on behalf of the United States Government assumes any liability resulting from the use of the information contained in this document, or warrants that such use will be free from privately owned rights.





## Light-Driven Polymeric Bimorph Actuators

Simple, relatively-low-power actuators could be integrated into MEMS and MEOMS.

John H. Glenn Research Center, Cleveland, Ohio

Light-driven polymeric bimorph actuators are being developed as alternatives to prior electrically and optically driven actuators in advanced, highly miniaturized devices and systems exemplified by microelectromechanical systems (MEMS), micro-electro-optical-mechanical systems (MEOMS), and sensor and actuator arrays in “smart” structures. These light-driven polymeric bimorph actuators are intended to satisfy a need for actuators that (1) in comparison with the prior actuators, are simpler and less power-hungry; (2) can be driven by low-power visible or mid-infrared light delivered through conventional optic fibers; and (3) are suitable for integration with optical sensors and multiple actuators of the same or different type.

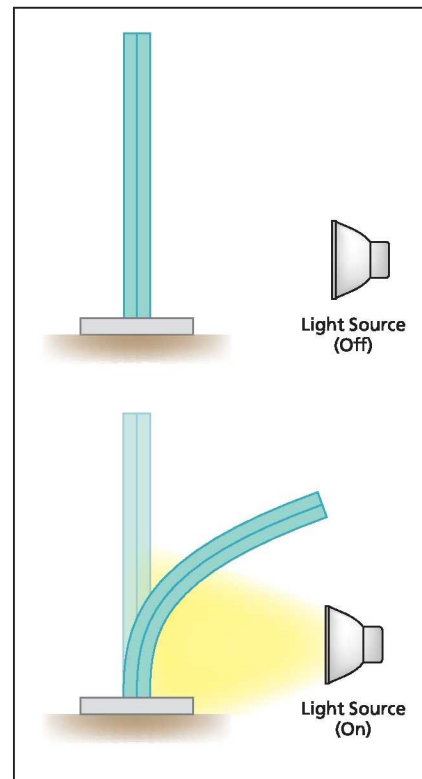
The immediate predecessors of the present light-driven polymeric bimorph actuators are bimorph actuators that exploit a photostrictive effect in lead lanthanum zirconate titanate (PLZT) ceramics. The disadvantages of the PLZT-based actuators are that (1) it is difficult to shape the PLZT ceramics, which are hard and brittle; (2) for actuation, it is necessary to use ultraviolet light (wavelengths < 380 nm), which must be generated by use of high-power, high-pressure arc lamps or lasers; (3) it is difficult to deliver sufficient ultraviolet light through conventional optical fibers because of significant losses in the fibers; (4) the response times of the PLZT actuators are of the order of several seconds — unacceptably long for typical applications; and (5) the maximum mechanical displacements of the PLZT-based actuators are limited to those characterized by low strains beyond which PLZT ceramics disintegrate because of their brittleness.

The basic element of a light-driven bimorph actuator of the present development type is a cantilever beam comprising two layers, at least one of which is a polymer that exhibits a photomechanical effect (see figure). The dominant mechanism of the photomechanical effect is a photothermal one: absorption of light energy causes heating, which, in turn, causes thermal expansion. The lay-

ers are made thin enough that the difference in temperature between the two layers in the presence of illumination is negligible. If the materials in the two layers are tailored to exhibit different degrees of the photomechanical effect, then the two layers undergo differential expansion when illuminated. As in other bimorph actuators, the differential expansion causes bending of the cantilever, and this bending constitutes the desired actuation. When the illumination is turned off, the illuminated spot cools and the cantilever returns to its previous shape. The typical response time of the photothermal mechanism is of the order of milliseconds, and the magnitude of the effect is relatively large (characterized by a strain of as much as 1 percent or greater).

One suitable photosensitive polymer is poly(vinylidene fluoride) [PVDF], which, heretofore, has been better known as a piezoelectric material. Processing conditions used in fabricating the two layers from PVDF or other polymer(s) can be chosen so that the coefficients of thermal expansion of the two layers differ by a significant amount, as needed to obtain the desired differential expansion. This polymer is flexible and, in comparison with PLZT ceramics, can be made to produce greater maximum strain using less light power. This polymer can be shaped by use of a variety of techniques, including molding, stamping, bending, cutting, and rolling. This polymer is also suitable for such thin-film techniques as spin casting, spraying, dipping, vapor deposition, contact printing, and photolithography that would be used in fabricating MEMS and MEOMS containing actuators of the present type.

The visible or infrared light needed to drive actuators of this type can be delivered via conventional communication-type optical fibers without incurring large losses like those of ultraviolet light needed to drive PLZT-based actuators. Lenses and/or other optical components can be used in conjunction with the optical fibers to shape the light



The Cantilever Beam depicted here comprises two layers that exhibit different degrees of a photomechanical effect. Consequently, illumination causes differential expansion that, in turn, causes bending of the beam.

beams and focus them at specific locations along actuator cantilevers as need for specific applications. Optionally, by use of a suitable number of optical fibers and lenses, light can be delivered to an actuator at one or more locations in pulses, and the pulses can be shaped and timed to cause the actuator to execute a desired trajectory.

*This work was done by Gregory Adamovsky of Glenn Research Center and Sergey S. Sarkisov and Michael J. Curley of Alabama A&M University. Further information is contained in a TSP (see page 1).*

*Inquiries concerning rights for the commercial use of this invention should be addressed to NASA Glenn Research Center, Innovative Partnerships Office, Attn: Steve Fedor, Mail Stop 4-8, 21000 Brookpark Road, Cleveland, Ohio 44135. Refer to LEW-17473-1.*

---

## ▶ **Guaranteeing Failsafe Operation of Extended-Scene Shack-Hartmann Wavefront Sensor Algorithm**

**Fast analysis rejects frames at the first sign of unacceptable quality instead of waiting until the full analysis is complete.**

*NASA's Jet Propulsion Laboratory, Pasadena, California*

A Shack-Hartmann sensor (SHS) is an optical instrument consisting of a lenslet array and a camera. It is widely used for wavefront sensing in optical testing and astronomical adaptive optics. The camera is placed at the focal point of the lenslet array and points at a star or any other point source. The image captured is an array of spot images. When the wavefront error at the lenslet array changes, the position of each spot measurably shifts from its original position. Determining the shifts of the spot images from their reference points shows the extent of the wavefront error.

An adaptive cross-correlation (ACC) algorithm has been developed to use scenes as well as point sources for wavefront error detection. Qualifying an extended scene image is often not an easy task due to changing conditions in scene

content, illumination level, background, Poisson noise, read-out noise, dark current, sampling format, and field of view. The proposed new technique based on ACC algorithm analyzes the effects of these conditions on the performance of the ACC algorithm and determines the viability of an extended scene image. If it is viable, then it can be used for error correction; if it is not, the image fails and will not be further processed. By potentially testing for a wide variety of conditions, the algorithm's accuracy can be virtually guaranteed.

In a typical application, the ACC algorithm finds image shifts of more than 500 Shack-Hartmann camera sub-images relative to a reference sub-image or cell when performing one wavefront sensing iteration. In the proposed new technique, a

pair of test and reference cells is selected from the same frame, preferably from two well-separated locations. The test cell is shifted by an integer number of pixels, say, for example, from  $m=-5$  to 5 along the  $x$ -direction by choosing a different area on the same sub-image, and the shifts are estimated using the ACC algorithm. The same is done in the  $y$ -direction. If the resulting shift estimate errors are less than a pre-determined threshold (e.g., 0.03 pixel), the image is accepted. Otherwise, it is rejected.

*This work was done by Erkin Sidick of Caltech for NASA's Jet Propulsion Laboratory.*

*The software used in this innovation is available for commercial licensing. Please contact Karina Edmonds of the California Institute of Technology at (626) 395-2322. Refer to NPO-46582.*

---

## ⊗ **Cloud Water Content Sensor for Sounding Balloons and Small UAVs**

*Goddard Space Flight Center, Greenbelt, Maryland*

A lightweight, battery-powered sensor was developed for measuring cloud water content, which is the amount of liquid or solid water present in a cloud, generally expressed as grams of water per cubic meter. This sensor has near-zero power consumption and can be flown on stan-

dard sounding balloons and small, unmanned aerial vehicles (UAVs).

The amount of solid or liquid water is important to the study of atmospheric processes and behavior. Previous sensing techniques relied on strongly heating the incoming air, which requires a major

energy input that cannot be achieved on sounding balloons or small UAVs.

*This work was done by John A. Bognar of Anasphere, Inc. for Goddard Space Flight Center. For further information, contact the Goddard Innovative Partnerships Office at (301) 286-5810. GSC-15638-1*

---

## ⊗ **Pixelized Device Control Actuators for Large Adaptive Optics**

**This technology can be used in military surveillance and relay mirrors, imaging for retinal disease, reconnaissance mapping, and missile detection and targeting.**

*Goddard Space Flight Center, Greenbelt, Maryland*

A fully integrated, compact, adaptive space optic mirror assembly has been developed, incorporating new advances in ultralight, high-performance composite mirrors. The composite mirrors use Q-switch matrix architecture-based pixelized control (PMN-PT) actuators, which achieve high-performance, large adaptive optic capability, while reduc-

ing the weight of present adaptive optic systems.

The self-contained, fully assembled, 11×11×4-in. (≈28×28×10-cm) unit integrates a very-high-performance 8-in. (≈20-cm) optic, and has 8-kHz true bandwidth. The assembled unit weighs less than 15 pounds (≈6.8 kg), including all mechanical assemblies, power elec-

tronics, control electronics, drive electronics, face sheet, wiring, and cabling. It requires just three wires to be attached (power, ground, and signal) for full-function systems integration, and uses a steel-frame and epoxied electronics. The three main innovations are:

1. Ultralightweight composite optics: A new replication method for fabrica-

tion of very thin composite 20-cm-diameter laminate face sheets with good as-fabricated optical figure was developed. The approach is a new mandrel resin surface deposition onto previously fabricated thin composite laminates.

2. Matrix (regenerative) power topology: Waveform correction can be achieved across an entire face sheet at 6 kHz, even for large actuator

counts. In practice, it was found to be better to develop a quadrant drive, that is, four quadrants of 169 actuators behind the face sheet. Each quadrant has a single, small, regenerative power supply driving all 169 actuators at 8 kHz in effective parallel.

3. Q-switch drive architecture: The Q-switch innovation is at the heart of the matrix architecture, and allows

for a very fast current draw into a desired actuator element in 120 counts of a MHz clock without any actuator coupling.

*This work was done by Gareth J. Knowles, Ross W. Bird, and Brian Shea of QorTek and Peter Chen of the Catholic University of America for Goddard Space Flight Center. For further information, contact the Goddard Innovative Partnerships Office at (301) 286-5810. GSC-15666-1*

## T-Slide Linear Actuators

**These long-stroke linear slide actuators can hold their position with power off.**

*Goddard Space Flight Center, Greenbelt, Maryland*

T-slide linear actuators use gear bearing differential epicyclic transmissions (GBDETs) to directly drive a linear rack, which, in turn, performs the actuation. Conventional systems use a rotary power source in conjunction with a nut and screw to provide linear motion. Non-back-drive properties of GBDET's make the new actuator more direct and simpler. Versions of this approach will serve as a long-stroke, ultra-precision, position actuator for NASA science instruments, and as a rugged, linear actuator for NASA deployment duties.

The T slide can operate effectively in the presence of side forces and torques. Versions of the actuator can perform ultra-precision positioning. A basic T-slide actuator is a long-stroke, rack-and-pinion linear actuator that, typically, consists of a T slide, several idlers, a transmission to drive the slide (powered by an electric motor) and a housing that holds the entire assembly. The actuator is driven by gear action on its top surface, and is guided and constrained by gear-bearing idlers on its other two parallel surfaces.

The geometry, implemented with gear-bearing technology, is particularly effective. An electronic motor operating

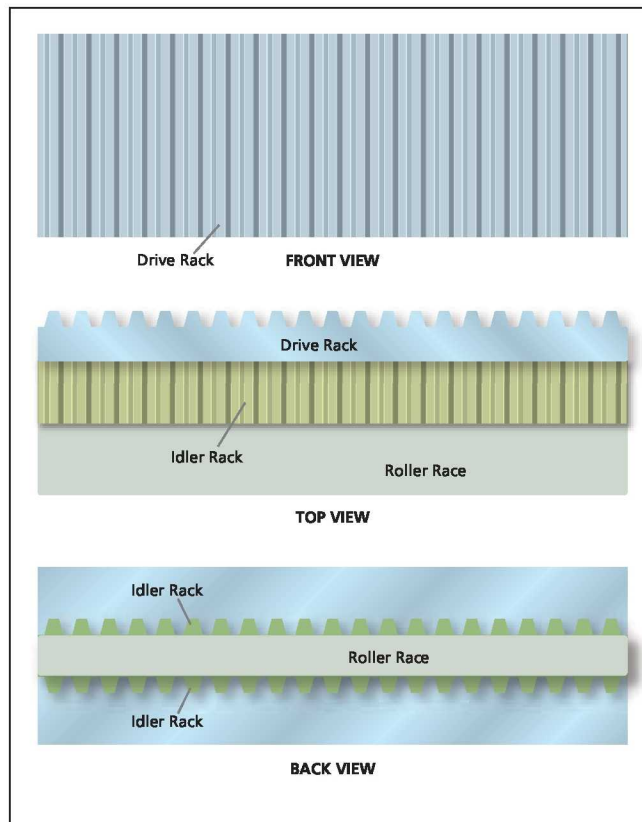
through a GBDET can directly drive the T slide against large loads, as a rack and pinion linear actuator, with no break and no danger of back driving. The actuator drives the slide into position and stops. The slide holds position with

power off and no brake, regardless of load. With the T-slide configuration, this GBDET has an entire T-gear surface on which to operate. The GB idlers coupling the other two T slide parallel surfaces to their housing counterpart surfaces provide constraints in five degrees-of-freedom and rolling friction in the direction of actuation. Multiple GB idlers provide roller bearing strength sufficient to support efficient, rolling friction movement, even in the presence of large, resisting forces.

T-slide actuators can be controlled using the combination of an off-the-shelf, electric servomotor, a motor angle resolution sensor (typically an encoder or resolver), and microprocessor-based intelligent software. In applications requiring precision positioning, it may be necessary to add strain gauges to the T-slide housing. Existing sensory-interactive motion control art will work for T slides.

For open-loop positioning, a stepping motor emulation technique can be used.

*This work was done by John Vranish of Goddard Space Flight Center. Further information is contained in a TSP (see page 1). GSC-15023-1*



Front, top, and back views of the T Slide and Idlers. The slide is driven by gear action on its top surface and is guided by gear-bearing idlers on its other two parallel surfaces.





## G<sup>4</sup>FET Implementations of Some Logic Circuits

One circuit can be made to perform multiple logic functions.

NASA's Jet Propulsion Laboratory, Pasadena, California

Some logic circuits have been built and demonstrated to work substantially as intended, all as part of a continuing effort to exploit the high degrees of design flexibility and functionality of the electronic devices known as G<sup>4</sup>FETs and described below. These logic circuits are intended to serve as prototypes of more-complex advanced programmable-logic-device-type integrated circuits, including field-programmable gate arrays (FPGAs). In comparison with prior FPGAs, these advanced FPGAs could be much more efficient because the functionality of G<sup>4</sup>FETs is such that fewer discrete components are needed to perform a given logic function in G<sup>4</sup>FET circuitry than are needed perform the same logic function in conventional transistor-based circuitry. The underlying concept of using G<sup>4</sup>FETs as building blocks of programmable logic circuitry was also described, from a different perspective, in "G<sup>4</sup>FETs as Universal and Programmable Logic Gates" (NPO-41698), *NASA Tech Briefs*, Vol. 31, No. 7 (July 2007), page 44.

A G<sup>4</sup>FET can be characterized as an accumulation-mode silicon-on-insulator (SOI) metal oxide/semiconductor field-effect transistor (MOSFET) featuring two junction field-effect transistor (JFET) gates. The structure of a G<sup>4</sup>FET (see Figure 1) is the same as that of a p-channel inversion-mode SOI MOSFET with two body contacts on each side of the channel. The top gate (G1), the substrate emulating a back gate (G2), and the junction gates (JG1 and JG2) can be biased independently of each other and, hence, each can be used to independently control some aspects of the conduction characteristics of the transistor. The independence of the actions of the four gates is what affords the enhanced functionality and design flexibility of G<sup>4</sup>FETs.

The present G<sup>4</sup>FET logic circuits include an adjustable-threshold inverter, a real-time-reconfigurable logic gate, and a dynamic random-access memory (DRAM) cell (see Figure 2). The configuration of the adjustable-threshold in-

verter is similar to that of an ordinary complementary metal oxide semiconductor (CMOS) inverter except that an NMOSFET (a MOSFET having an n-doped channel and a p-doped Si substrate) is replaced by an n-channel G<sup>4</sup>FET. The side gates (JG1 and JG2) are used to linearly modulate the threshold voltage of the G<sup>4</sup>FET, thereby

modulating the switching threshold voltage of the inverter. By judiciously selecting the design and operational parameters that affect the switching threshold voltage, the inverter can be made to function as a quaternary down literal converter. (The term "down literal converter" denotes a circuit that performs a function, known as the down

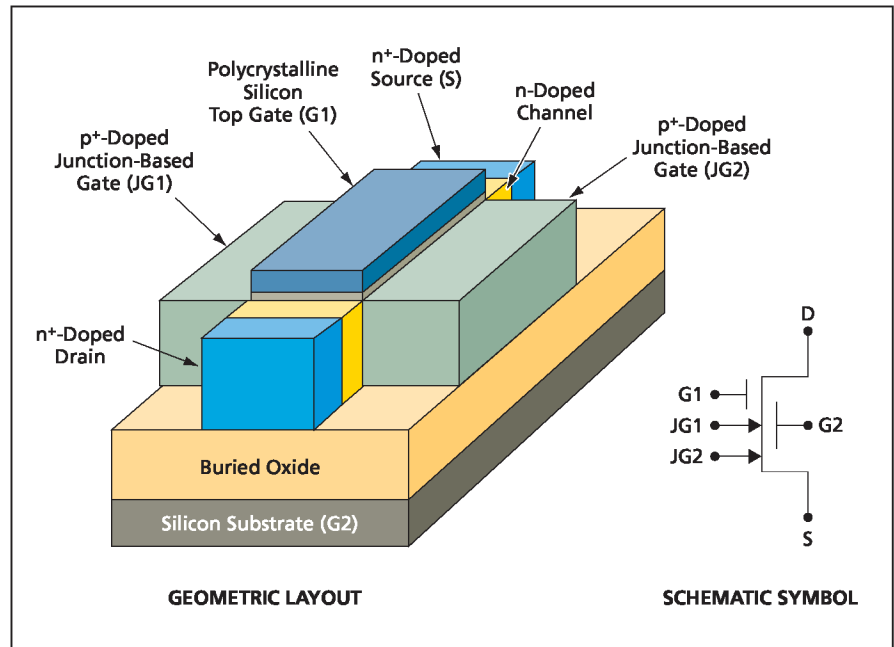


Figure 1. In a G<sup>4</sup>FET, the four gates (G1, G2, JG1, and JG2) can be biased independently. JG1 and JG2 can be considered as extra gates that provide additional degrees of freedom for design and operation, beyond those of a conventional MOSFET.

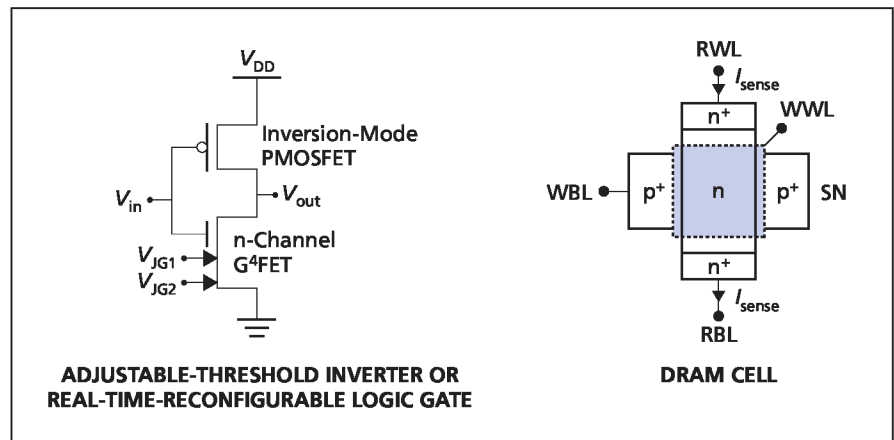


Figure 2. These G<sup>4</sup>FET Logic Circuits can be building blocks of complex programmable logic devices.

literal function, that is the fundamental element in multi-valued logic.) Hence, the adjustable-threshold inverter can be made a basic building block of quaternary logic circuits.

The real-time-reconfigurable logic gate can be realized, in a circuit partly resembling the adjustable-threshold inverter, by applying the logic input signals to JG1 and JG2 and connecting the input terminal of what would otherwise be the inverter to a constant reference voltage (that is, making  $V_{in}$  a constant voltage). The number of transistors in this circuit is smaller than in a classical CMOS circuit that performs an equivalent logic function. The same hardware can be made to form any of three different functions: Depending on the value of  $V_{in}$ , the function is disabled output ( $V_{out} = V_{DD}$  or 0), the NOR of the logic levels represented by  $V_{JG1}$  and  $V_{JG2}$ , or

the NAND of the logic levels represented by  $V_{JG1}$  and  $V_{JG2}$ .

In the DRAM cell, the lateral inversion-mode PMOSFET (a MOSFET having a p-doped channel and an n-doped Si substrate) inherent in the n-channel  $G^4$ FET is used for writing data in the horizontal direction, while the p-channel JFET serves to read the data in the vertical direction. When the WWL signal turns on the PMOS switch, the potential of the storage node (SN) is modulated by WBL. When writing is disabled, SN is isolated, and during the retention time, its depletion region is more or less extended toward the body, depending on value of the datum stored in it. As a result, the resistance of the JFET channel in the vertical direction is affected, causing the sensing current ( $I_{sense}$ ) to be a function of the stored data. The sensing-current char-

acteristics can be optimized via the layout of the  $G^4$ FET structure.

*This work was done by Mohammad Mojaradi of Caltech; Kerem Akarvardar, Sorin Cristoleveanu, and Paul Gentil of Grenoble University; and Benjamin Blalock and Suhan Chen of University of Tennessee for NASA's Jet Propulsion Laboratory.*

*In accordance with Public Law 96-517, the contractor has elected to retain title to this invention. Inquiries concerning rights for its commercial use should be addressed to:*

*Innovative Technology Assets Management  
JPL*

*Mail Stop 202-233  
4800 Oak Grove Drive  
Pasadena, CA 91109-8099  
(818) 354-2240*

*E-mail: iaoffice@jpl.nasa.gov*

*Refer to NPO-44007, volume and number of this NASA Tech Briefs issue, and the page number.*

## Electrically Variable or Programmable Nonvolatile Capacitors

Capacitances are measured using small AC signals or changed using larger pulses.

Marshall Space Flight Center, Alabama

Electrically variable or programmable capacitors based on the unique properties of thin perovskite films are undergoing development. These capacitors show promise of overcoming two important deficiencies of prior electrically programmable capacitors:

- Unlike in the case of varactors, it is not necessary to supply power continuously to make these capacitors retain their capacitance values. Hence, these capacitors may prove useful as components of nonvolatile analog and digital electronic memories.
- Unlike in the case of ferroelectric capacitors, it is possible to measure the capacitance values of these capacitors without changing the values. In other words, whereas readout of ferroelectric capacitors is destructive, readout of these capacitors can be nondestructive.

A capacitor of this type is a simple two-terminal device. It includes a thin film of a suitable perovskite as the dielectric layer, sandwiched between two metal or metal oxide electrodes (for example, see Figure 1). The utility of this device as a variable capacitor is based on a phenomenon, known as electrical-pulse-induced capacitance (EPIC), that is observed in thin perovskite films and especially in those thin perovskite films that exhibit the colossal magnetoresistive (CMR) ef-

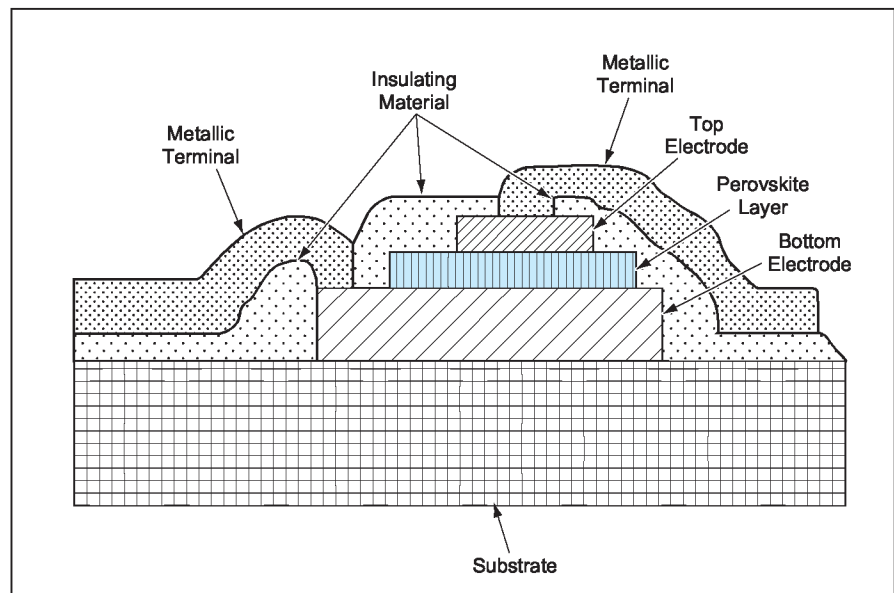


Figure 1. An Electrically Variable Capacitor of the type described in the text can be fabricated on a silicon or other substrate as part of an integrated circuit.

fect. In EPIC, the application of one or more electrical pulses that exceed a threshold magnitude (typically somewhat less than 1 V) gives rise to a nonvolatile change in capacitance. The change in capacitance depends on the magnitude duration, polarity, and number of pulses. It is not necessary to apply a magnetic field or to cool the device

below (or heat it above) room temperature to obtain EPIC. Examples of suitable CMR perovskites include  $Pr_{1-x}Ca_xMnO_3$ ,  $La_{1-x}Ca_xMnO_3$ ,  $La_{1-x}Sr_xMnO_3$ , and  $Nb_{1-x}Ca_xMnO_3$ .

Figure 2 is a block diagram showing an EPIC capacitor connected to a circuit that can vary the capacitance, measure the capacitance, and/or measure the re-

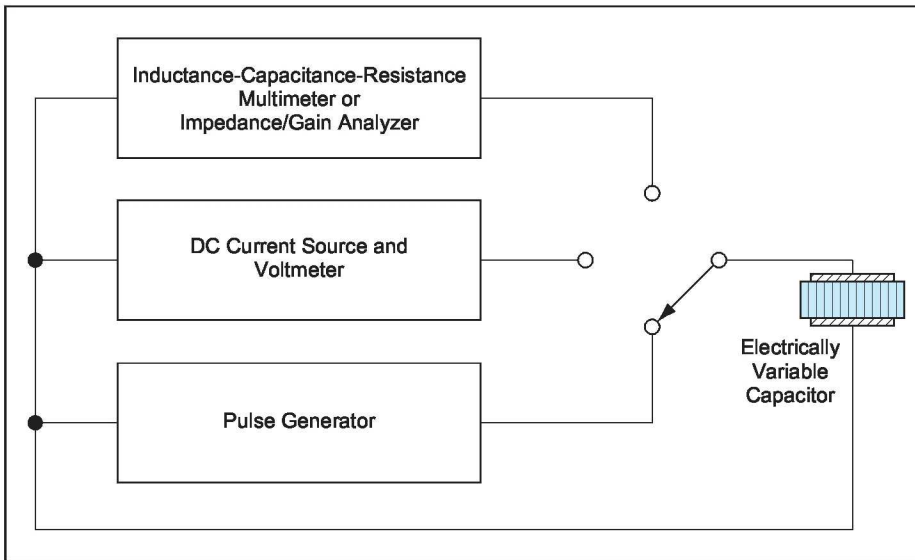


Figure 2. The Capacitance of the Electrically Variable Capacitor is changed or measured, depending on the position of the switch and the nature of the applied signal.

sistance of the capacitor. A pulse generator applies voltage pulses to change the capacitance. If desired, after each pulse, the capacitance and resistance can be measured by use of an inductance-capacitance-resistance multimeter or an impedance/gain analyzer. Also if desired, the DC resistance can be measured by applying a current of  $\approx 1 \mu\text{A}$  and measur-

ing the resulting voltage drop between the electrodes by use of a high-internal-resistance voltmeter. The magnitude of the AC test potential applied by the multimeter or analyzer and/or the magnitude of the DC test potential is kept below 50 mV — well below the threshold magnitude — so as not to change the capacitance unintentionally.

The threshold potential depends on a number of factors, including the composition and thickness of the perovskite film and the details of the process used to fabricate the device. The change in capacitance caused by a given pulse can be wholly or partly reversed by reversing the polarity of the pulse: that is, a pulse with one polarity causes the capacitance to decrease, and a pulse of the opposite polarity causes the capacitance to increase. The sign of the change in capacitance in relation to polarity of a pulse depends on the aforementioned factors and on additional factors, including the capacitance-change history of the device, the amplitude and duration of the pulse. After each change, the capacitance value is stable: It remains the same after repeated measurements using a signal much smaller than a capacitance-changing pulse.

*This work was done by Shangqing Liu, Naijuan Wu, Alex Ignatiev, and Jianren Li of the University of Houston for Marshall Space Flight Center. For more information, contact Sammy Nabors, MSFC Commercialization Assistance Lead, at sammy.a.nabors@nasa.gov. Refer to MFS-31960-1*

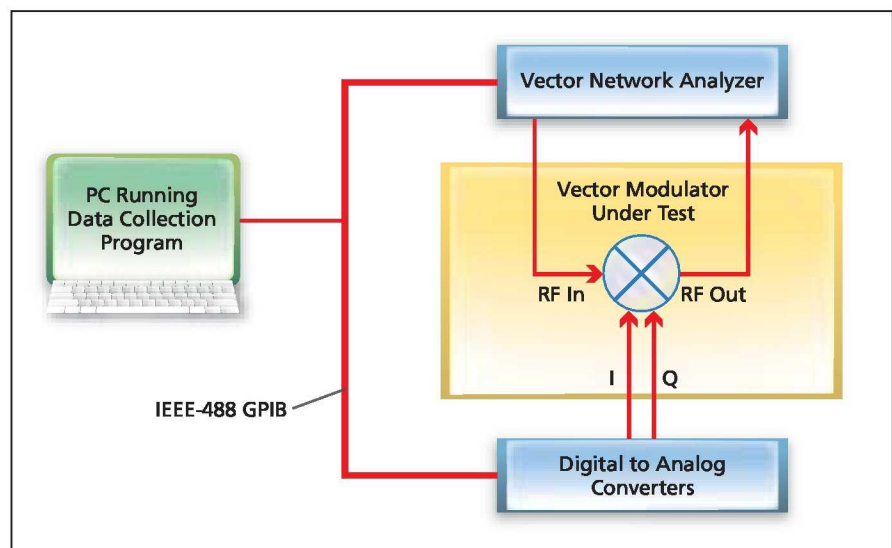
## System for Automated Calibration of Vector Modulators

**This test system helps create tabular or algorithmic functions to compensate for non-ideal behavior in vector modulators.**

*NASA's Jet Propulsion Laboratory, Pasadena, California*

Vector modulators are used to impose baseband modulation on RF signals, but non-ideal behavior limits the overall performance. The non-ideal behavior of the vector modulator is compensated using data collected with the use of an automated test system driven by a LabVIEW<sup>®</sup> program that systematically applies thousands of control-signal values to the device under test and collects RF measurement data.

The technology innovation automates several steps in the process. First, an automated test system, using computer-controlled digital-to-analog converters (DACs) and a computer-controlled vector network analyzer (VNA) systematically can apply different I and Q signals (which represent the complex number by which the RF signal is multiplied) to the vector modulator under test (VMUT), while measuring the RF per-



The Automated Test System uses computer-controlled digital-to-analog converters and a VNA to systematically apply I and Q signals to the VMUT, while measuring the RF performance.

formance — specifically, gain and phase (see figure). The automated test system uses the LabVIEW software to control the test equipment, collect the data, and write it to a file. The input to the LabVIEW program is either user-input for systematic variation, or is provided in a file containing specific test values that should be fed to the VMUT. The output file contains both the control signals and the measured data.

The second step is to post-process the file to determine the correction functions as needed. The result of the entire process is a tabular representation, which allows translation of a desired I/Q value to the required analog control signals to produce a particular RF behavior. In some applications, “corrected” perform-

ance is needed only for a limited range. If the vector modulator is being used as a phase shifter, there is only a need to correct I and Q values that represent points on a circle, not the entire plane.

This innovation has been used to calibrate 2-GHz MMIC (monolithic microwave integrated circuit) vector modulators in the High EIRP Cluster Array project (EIRP is high effective isotropic radiated power). These calibrations were then used to create correction tables to allow the commanding of the phase shift in each of four channels used as a phased array for beam steering of a Ka-band (32-GHz) signal.

The system also was the basis of a breadboard electronic beam steering system. In this breadboard, the goal was

not to make systematic measurements of the properties of a vector modulator, but to drive the breadboard with a series of test patterns varying in phase and amplitude. This is essentially the same calibration process, but with the difference that the data collection process is oriented toward collecting breadboard performance, rather than the measurement of output from a network analyzer.

*This work was done by James Lux, Amy Boas, and Samuel Li of Caltech for NASA’s Jet Propulsion Laboratory. Further information is contained in a TSP (see page 1).*

*The software used in this innovation is available for commercial licensing. Please contact Karina Edmonds of the California Institute of Technology at (626) 395-2322. Refer to NPO-44518.*

## Complementary Paired G<sup>4</sup>FETs as Voltage-Controlled NDR Device

G<sup>4</sup>FET-based NDR circuits are more versatile than their predecessors.

NASA’s Jet Propulsion Laboratory, Pasadena, California

It is possible to synthesize a voltage-controlled negative-differential-resistance (NDR) device or circuit by use of a pair of complementary G<sup>4</sup>FETs (four-gate field-effect transistors). [For more information about G<sup>4</sup>FETs, please see the immediately preceding article.] As shown in Figure 1, the present voltage-controlled NDR device or circuit is an updated version of a prior NDR device or circuit, known as a lambda diode, that contains a pair of complementary junction field-effect transistors (JFETs). (The lambda diode is so named because its current-versus-voltage plot bears some resemblance to an upper-case lambda.) The present version can be derived from the prior version by substituting G<sup>4</sup>FETs for the JFETs and connecting both JFET gates of each G<sup>4</sup>FET together. The front gate terminals

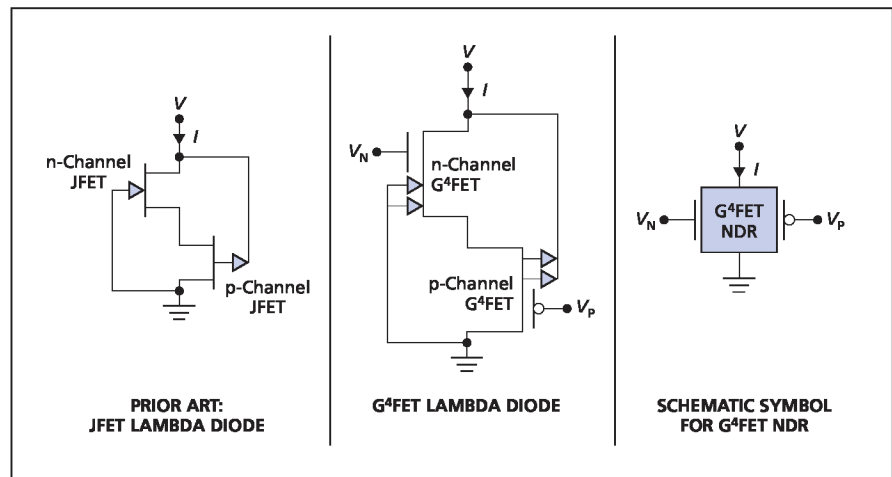


Figure 1. A Lambda Diode is a negative-resistance circuit or device, previously made from JFETs, and now made from G<sup>4</sup>FETs.

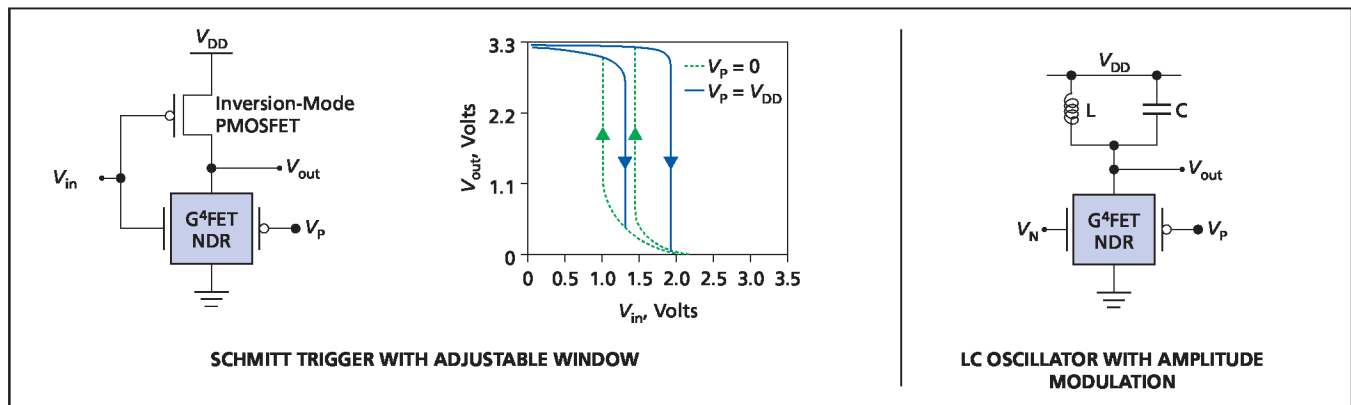


Figure 2. This LC Oscillator and Schmitt Trigger are examples of enhanced NDR circuits that can be made by use of G<sup>4</sup>FETs.

of the G<sup>4</sup>FETs constitute additional terminals (that is, terminals not available in the older JFET version) to which one can apply control voltages  $V_N$  and  $V_P$ .

Circuits in which NDR devices have been used include (1) Schmitt triggers and (2) oscillators containing inductance/capacitance (LC) resonant circuits. Figure 2 depicts such circuits containing G<sup>4</sup>FET NDR devices like that of Figure 1. In the Schmitt trigger shown here, the G<sup>4</sup>FET NDR is loaded with an ordinary inversion-mode, p-channel, metal oxide/semiconductor field-effect transistor (inversion-mode PMOSFET), the  $V_N$  terminal of the G<sup>4</sup>FET NDR device is used as an input terminal, and the input terminals of the PMOSFET and the G<sup>4</sup>FET NDR device are connected.  $V_P$  can be used as an extra control volt-

age (that is, a control voltage not available in a typical prior Schmitt trigger) for adjusting the pinch-off voltage of the p-channel G<sup>4</sup>FET and thereby adjusting the trigger-voltage window.

In the oscillator, a G<sup>4</sup>FET NDR device is loaded with a conventional LC tank circuit. As in other LC NDR oscillators, oscillation occurs because the NDR counteracts the resistance in the tank circuit. The advantage of this G<sup>4</sup>FET-NDR LC oscillator over a conventional LC NDR oscillator is that one can apply a time-varying signal to one of the extra control input terminals ( $V_N$  or  $V_P$ ) to modulate the conductance of the NDR device and thereby amplitude-modulate the output signal.

*This work was done by Mohammad Mojaradi of Caltech; Suheng Chen, Ben Blalock, Chuck Britton, Ben Prothro, and James Vander-*

*sand of the University of Tennessee; Ron Schrimph of Vanderbilt University; and Sorin Cristoloveanu, Kerem Akarvardar, and P. Gentil of Grenoble University for NASA's Jet Propulsion Laboratory. Further information is contained in a TSP (see page 1).*

*In accordance with Public Law 96-517, the contractor has elected to retain title to this invention. Inquiries concerning rights for its commercial use should be addressed to:*

*Innovative Technology Assets Management*

*JPL*

*Mail Stop 202-233*

*4800 Oak Grove Drive*

*Pasadena, CA 91109-8099*

*(818) 354-2240*

*E-mail: iaoffice@jpl.nasa.gov*

*Refer to NPO-43929, volume and number of this NASA Tech Briefs issue, and the page number.*

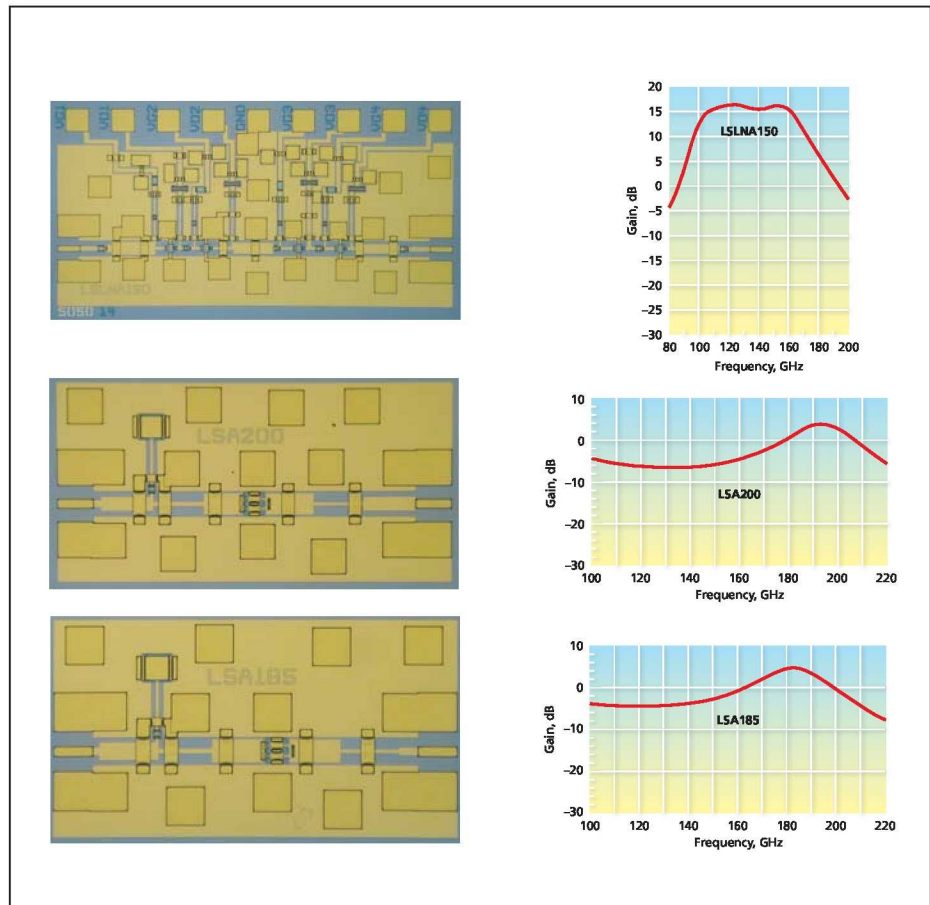
## Three MMIC Amplifiers for the 120-to-200 GHz Frequency Band

These would complement previously reported MMIC amplifiers designed for overlapping frequency bands.

NASA's Jet Propulsion Laboratory, Pasadena, California

Closely following the development reported in the immediately preceding article, three new monolithic microwave integrated circuit (MMIC) amplifiers that would operate in the 120-to-200-GHz frequency band have been designed and are under construction at this writing. The active devices in these amplifiers are InP high-electron-mobility transistors (HEMTs). These amplifiers (see figure) are denoted the LSLNA150, the LSA200, and the LSA185, respectively.

Like the amplifiers reported in the immediately preceding article, the LSLNA150 (1) is intended to be a prototype of low-noise amplifiers (LNAs) to be incorporated into spaceborne instruments for sensing cosmic microwave background radiation and (2) has potential for terrestrial use in electronic test equipment, passive millimeter-wave imaging systems, radar receivers, communication receivers, and systems for detecting hidden weapons. The HEMTs in this amplifier were fabricated according to 0.08- $\mu\text{m}$  design rules of a commercial product line of InP HEMT MMICs at HRL Laboratories, LLC, with a gate geometry of 2 fingers, each 15  $\mu\text{m}$  wide. On the basis of computational simulations, this amplifier is designed to afford at least 15



These Three MMIC Amplifiers have been designed to be suitable for a variety of applications at frequencies up to about 200 GHz.

dB of gain, with a noise figure of no more than about 6 dB, at frequencies from 120 to 160 GHz. The measured results of the amplifier are shown next to the chip photo, with a gain of 16 dB at 150 GHz. Noise figure work is ongoing.

The LSA200 and the LSA185 are intended to be prototypes of transmitting power amplifiers for use at frequencies between about 180 and about 200 GHz.

These amplifiers have also been fabricated according to rules of the aforesaid commercial product line of InP HEMT MMICs, except that the HEMTs in these amplifiers are characterized by a gate geometry of 4 fingers, each 37  $\mu\text{m}$  wide. The measured peak performance of the LSA200 is characterized by a gain of about 1.4 dB at a frequency of 190 GHz; the measured peak perform-

ance of the LSA185 is characterized by a gain of about 2.7 dB at a frequency of 181 GHz. The measured gain results of each chip are shown next to their respective photos.

*This work was done by Lorene Samoska of Caltech and Adele Schmitz of HRL Laboratories, LLC, for NASA's Jet Propulsion Laboratory. Further information is contained in a TSP (see page 1). NPO-42846*

## Low-Noise MMIC Amplifiers for 120 to 180 GHz

Potential applications include radar, communications, radiometry, and millimeter-wave imaging.

NASA's Jet Propulsion Laboratory, Pasadena, California

Three-stage monolithic millimeter-wave integrated-circuit (MMIC) amplifiers capable of providing useful amounts of gain over the frequency range from 120 to 180 GHz have been developed as prototype low-noise amplifiers (LNAs) to be incorporated into instruments for sensing cosmic microwave background radiation. There are also potential uses for such LNAs in electronic test equipment, passive millimeter-wave imaging systems, radar receivers, communication receivers, and systems for detecting hidden weapons. The main advantage afforded by these MMIC LNAs, relative to prior MMIC LNAs, is that their coverage of the 120-to-180-GHz frequency band makes them suitable for reuse in a wider variety of applications without need to redesign them. Each of these MMIC amplifiers includes InP transistors and coplanar waveguide circuitry on a 50- $\mu\text{m}$ -thick chip (see Figure 1). Coplanar waveguide transmission lines are used for both applying DC bias and matching of input and output impedances of each transistor stage. Via holes are incorporated between top and bottom ground planes to suppress propagation of electromagnetic modes in the substrate.

On the basis of computational simulations, each of these amplifiers was expected to operate with a small-signal gain of 14 dB and a noise figure of 4.3 dB. At the time of writing this article, measurements of noise figures had not been reported, but on-chip measurements had shown gains approaching their simulated values (see Figure 2).

*This work was done by David Pukala, Lorene Samoska, and Alejandro Peralta of Caltech and Brian Bayuk, Ron Grundbacher, Patricia Oliver, Abdullah Cavus, and Po-Hsin Liu of Northrop Grumman Corporation for NASA's Jet Propulsion Laboratory. Further information is contained in a TSP (see page 1). NPO-42783*

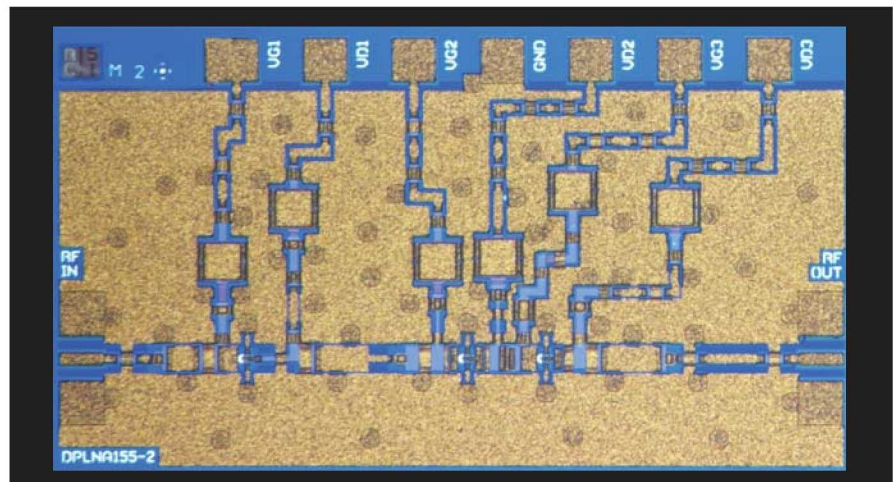


Figure 1. This MMIC contains three InP amplifier stages plus coplanar waveguide transmission lines for input and output impedance matching and DC biasing.

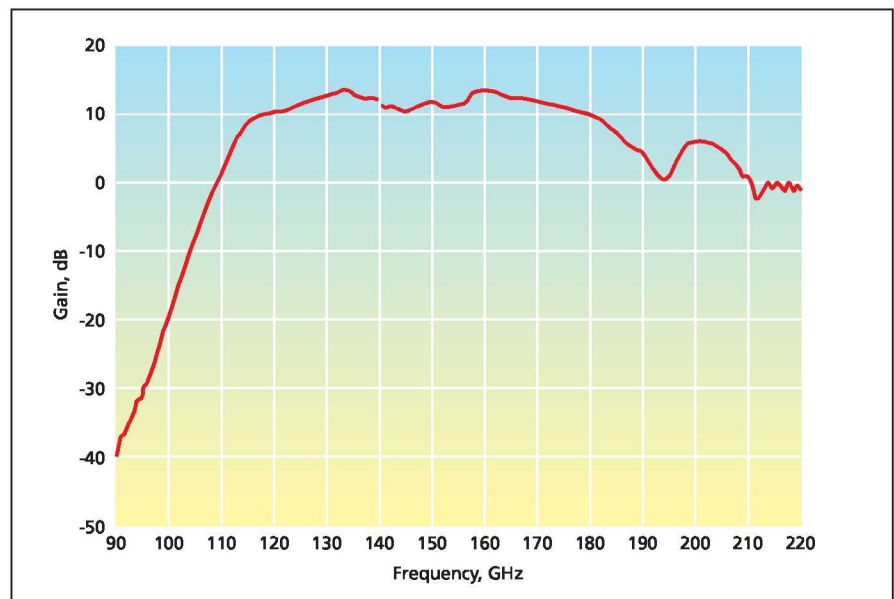


Figure 2. The Measured Gain of an amplifier like that shown in Figure 1 was found to exceed 10 dB over most of the frequency range from 120 to 180 GHz. The discontinuity in the plot at 140 GHz is an artifact of switching, at that frequency, between two waveguide bands of the instrumentation used to measure the gain.



## Using Ozone To Clean and Passivate Oxygen-Handling Hardware

Lyndon B. Johnson Space Center, Houston, Texas

A proposed method of cleaning, passivating, and verifying the cleanliness of oxygen-handling hardware would extend the established art of cleaning by use of ozone. As used here, "cleaning" signifies ridding all exposed surfaces of combustible (in particular, carbon-based) contaminants. The method calls for ex-

posing the surfaces of the hardware to ozone while monitoring the ozone effluent for carbon dioxide. The ozone would passivate the hardware while oxidizing carbon-based residues, converting the carbon in them to carbon dioxide. The exposure to ozone would be continued until no more carbon dioxide was de-

tected, signifying that cleaning and passivation were complete.

*This work was done by Paul Torrance of Johnson Space Center and Paul Biesinger of Science Applications International Corp. For further information, contact the Johnson Commercial Technology Office at (281) 483-3809. MSC-23290-1*

## Metal Standards for Waveguide Characterization of Materials

Metal waveguide inserts can be tailored to have known scattering parameters.

John H. Glenn Research Center, Cleveland, Ohio

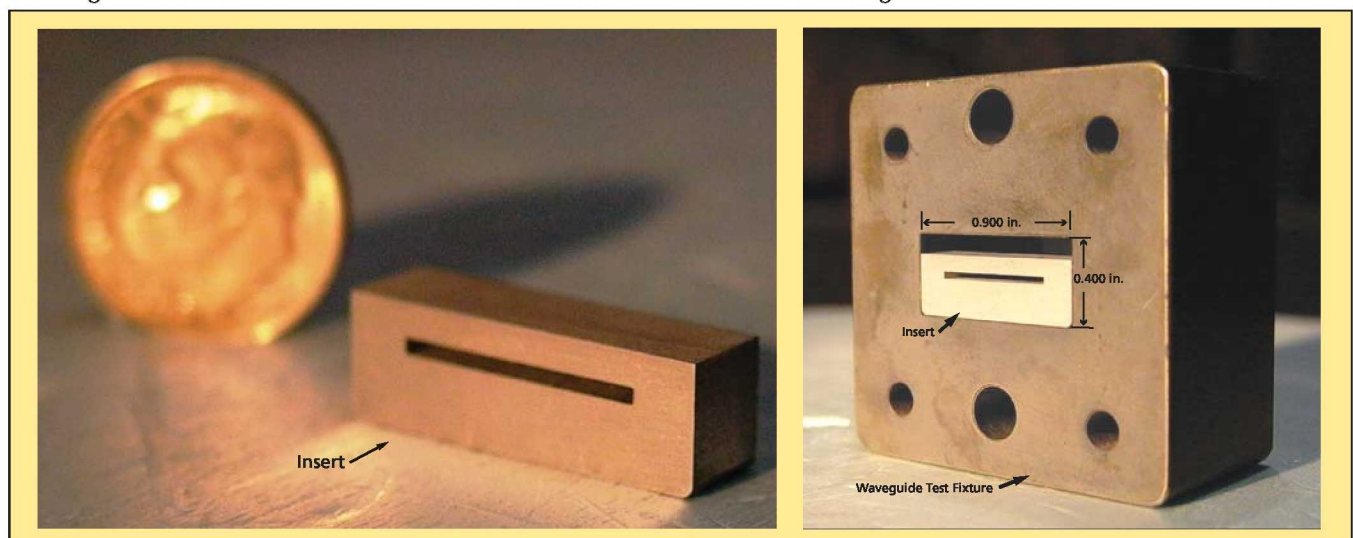
Rectangular-waveguide inserts that are made of non-ferromagnetic metals and are sized and shaped to function as notch filters have been conceived as reference standards for use in the rectangular-waveguide method of characterizing materials with respect to such constitutive electromagnetic properties as permittivity and permeability. Such standards are needed for determining the accuracy of measurements used in the method, as described below.

In this method, a specimen of a material to be characterized is cut to a prescribed size and shape and inserted in a rectangular-waveguide test fixture, wherein the

specimen is irradiated with a known source signal and detectors are used to measure the signals reflected by, and transmitted through, the specimen. Scattering parameters [also known as "S" parameters ( $S_{11}$ ,  $S_{12}$ ,  $S_{21}$ , and  $S_{22}$ )] are computed from ratios between the transmitted and reflected signals and the source signal. Then the permeability and permittivity of the specimen material are derived from the scattering parameters. Theoretically, the technique for calculating the permeability and permittivity from the scattering parameters is exact, but the accuracy of the results depends on the accuracy of the measurements from which the scattering

parameters are obtained. To determine whether the measurements are accurate, it is necessary to perform comparable measurements on reference standards, which are essentially specimens that have known scattering parameters.

To be most useful, reference standards should provide the full range of scattering-parameter values that can be obtained from material specimens. Specifically, measurements of the back-scattering parameter ( $S_{11}$ ) from no reflection to total reflection and of the forward-transmission parameter ( $S_{21}$ ) from no transmission to total transmission are needed. A reference standard



The Metal Rectangular-Waveguide Insert is sized and shaped to fit the waveguide cross-section and to act as a band-stop filter having a notch frequency of about 9 GHz. The particular waveguide cross sectional dimensions, known in the industry as "WR-90," are for a nominal frequency range of 8.2 to 12.4 GHz.

that functions as a notch (band-stop) filter can satisfy this need because as the signal frequency is varied across the frequency range for which the filter is designed, the scattering parameters vary over the ranges of values between the extremes of total reflection and total transmission.

A notch-filter reference standard in the form of a rectangular-waveguide insert that has a size and shape similar to that of a material specimen is advantageous because the measurement configuration used for the reference standard can be the same as that for a material specimen. Typically a speci-

men is a block of material that fills a waveguide cross-section but occupies only a small fraction of the length of the waveguide. A reference standard of the present type (see figure) is a metal block that fills part of a waveguide cross section and contains a slot, the long dimension of which can be chosen to tailor the notch frequency to a desired value. The scattering parameters and notch frequency can be estimated with high accuracy by use of commercially available electromagnetic-field-simulating software. The block can be fabricated to the requisite precision by wire electrical-discharge machining. In use,

the accuracy of measurements is determined by comparison of (1) the scattering parameters calculated from the measurements with (2) the scattering parameters calculated by the aforementioned software.

*This work was done by Kevin M. Lambert and Carol L. Kory of Analex Corp. for Glenn Research Center. Further information is contained in a TSP (see page 1).*

*Inquiries concerning rights for the commercial use of this invention should be addressed to NASA Glenn Research Center, Innovative Partnerships Office, Attn: Steve Fedor, Mail Stop 4-8, 21000 Brookpark Road, Cleveland, Ohio 44135. Refer to LEW-18137-1.*

## Two-Piece Screens for Decontaminating Granular Material

**These are more effective than are single-piece screens.**

*Marshall Space Flight Center, Alabama*

Two-piece screens have been designed specifically for use in filtering a granular material to remove contaminant particles that are significantly wider or longer than are the desired granules. In the original application for which the two-piece screens were conceived, the granular material is ammonium perchlorate and the contaminant particles tend to be wires and other relatively long, rigid strands. The basic design of the two-piece screens can be adapted to other granular materials and contaminants by modifying critical dimensions to accommodate different grain and contaminant-particle sizes.

A two-piece screen of this type consists mainly of (1) a top flat plate perforated with circular holes arranged in a hexagonal pattern and (2) a bottom plate that is also perforated with circular holes (but not in a pure hexagonal pattern) and is folded into an accordion structure. Fabrication of the bottom plate begins with drilling circular holes into a flat plate in a hexagonal pattern that is interrupted, at regular intervals, by parallel gaps. The plate is then

folded into the accordion structure along the gaps. Because the folds are along the gaps, there are no holes at the peaks and valleys of the accordion screen. The top flat plate and the bottom accordion plate are secured within a metal frame. The resulting two-piece screen is placed at the bottom opening of a feed hopper containing the granular material to be filtered.

Tests have shown that such long, rigid contaminant strands as wires readily can pass through a filter consisting of the flat screen alone and that the addition of the accordion screen below the flat screen greatly increases the effectiveness of removal of wires and other contaminant strands. Part of the reason for increased effectiveness is in the presentation of the contaminant to the filter surface. Testing has shown that wire type contamination will readily align itself parallel to the material direction flow. Since this direction of flow is nearly always perpendicular to the filter surface holes, the contamination is automatically aligned to pass through. The two-filter configuration reduces the likelihood that a given contam-

inant strand will be aligned with the flow of material by eliminating the perpendicular presentation angle. Thus, for wires of a certain diameter, a two-piece screen is 20 percent more effective than is the corresponding flat perforated plate alone, even if the holes in the flat plate are narrower.

An accordion screen alone is similarly effective in catching contaminants, but lumps of agglomerated granules of the desired material often collect in the valleys and clog the screen. The addition of a flat screen above the accordion screen prevents clogging of the accordion screen. Flat wire screens have often been used to remove contaminants from granular materials, and are about as effective as are the corresponding perforated flat plates used alone.

*This work was done by Douglas Backes, Clay Poulter, Max Godfrey, Melinda Dutton, and Dennis Tolman of Alliant Techsystems Inc. for Marshall Space Flight Center. For more information, contact Sammy Nabors, MSFC Commercialization Assistance Lead, at sammy.a.nabors@nasa.gov. Refer to MFS-32496-1*



## Mercuric Iodide Anticoincidence Shield for Gamma-Ray Spectrometer

*Goddard Space Flight Center, Greenbelt, Maryland*

A film-growth process was developed for polycrystalline mercuric iodide that creates cost-effective, large-area detectors for high-energy charged-particle detection. A material, called a barrier film, is introduced onto the substrate before the normal mercuric iodide film growth process. The barrier film improves the

quality of the normal film grown and enhances the adhesion between the film and the substrate.

The films grown using this improved technique were found to have adequate signal-to-noise properties so that individual high-energy charged-particle interactions could be distinguished from noise,

and thus, could be used to provide an anticoincidence veto function as desired.

*This work was done by Neal Hartsough and Jan Iwanczyk of DxRay, Inc. for Goddard Space Flight Center. For further information, contact the Goddard Innovative Partnerships Office at (301) 286-5810. GSC-15635-1*

## Improved Method of Design for Folding Inflatable Shells

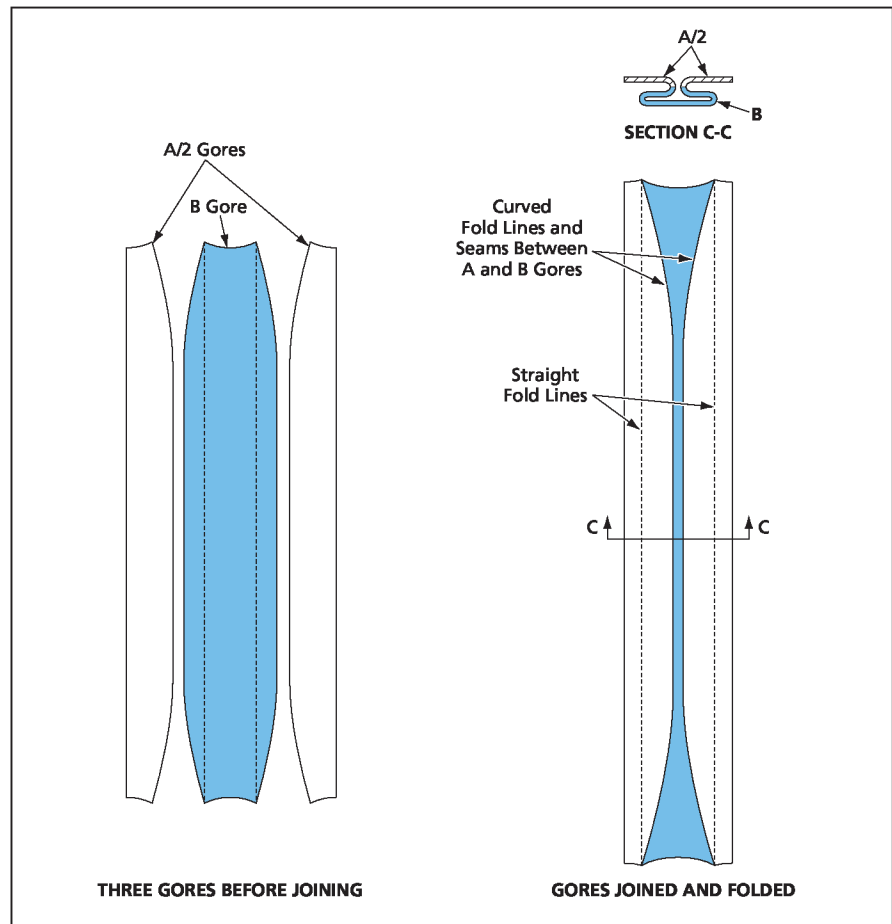
**Designs of gores reflect multiple considerations of assembly, stowage, and deployment.**

*Lyndon B. Johnson Space Center, Houston, Texas*

An improved method of designing complexly shaped inflatable shells to be assembled from gores was conceived for original application to the inflatable outer shell of a developmental habitable spacecraft module having a cylindrical mid-length section with toroidal end caps. The method is also applicable to inflatable shells of various shapes for terrestrial use.

The method addresses problems associated with the assembly, folding, transport, and deployment of inflatable shells that may comprise multiple layers and have complex shapes that can include such doubly curved surfaces as toroids and spheres. One particularly difficult problem is that of mathematically defining fold lines on a gore pattern in a double-curvature region. Moreover, because the fold lines in a double-curvature region tend to be curved, there is a practical problem of how to implement the folds. Another problem is that of modifying the basic gore shapes and sizes for the various layers so that when they are folded as part of the integral structure, they do not mechanically interfere with each other at the fold lines.

Heretofore, it has been a common practice to design an inflatable shell to be assembled in the deployed configuration, without regard for the need to fold it into compact form. Typically, the result has been that folding has been a difficult, time-consuming process resulting in a



The Basic Repeating Unit of a shell comprising a cylinder with toroidal end caps is a subassembly of three gores.

poor stowed configuration. Hence, yet another problem is to design the shell to be assembled in the stowed configuration, bypassing the folding process at the vehicle level.

The problem of weight relief can be summarized as one of securing the stowed shell against shifting under its own weight during transport, without imposing excessive stress on any part of the shell. The weight-relief problem may not be significant in all applications, but launch acceleration makes it so in the original spacecraft application.

To solve these problems, in the improved method, one does more than merely choose the sizes and shapes of the gores to obtain the specified deployed shape of a shell. In addition, one chooses the sizes and shapes of the gores and the fold lines, in conjunction with the sequence of incorporation of the gores, to enable assembly of the shell in the

stowed configuration, without interference between layers. To make this possible, the fold lines and the shapes of the gores are defined by equations that reflect the aforementioned problems and requirements. These equations incorporate the required modifications for the layers in each gore, accounting for the thicknesses of the layers and providing corresponding margins to prevent interference at fold lines.

The equations also provide for simplification of fold lines in double-curvature regions. For example, in the original application, the basic repeating unit for forming a cylinder with toroidal end caps consists of a gore designated B between two gores designated A/2, as shown in the figure. The B gore contains two straight fold lines that run the entire length, including the toroidal regions at the ends. The seams between the A/2 and B gores constitute a second pair of

fold lines that are curved in the end regions, the curvature being such as to enable the flat folded pattern to deploy to the desired toroidal shape at the ends. When repeating units are joined together at vehicle installation, adjacent A/2 gores become a full A gore.

The weight-relief problem is solved by use of straps attached between (1) suitably chosen locations near fold lines and (2) adjacent supporting fixtures on a rigid structure on which the folded shell is to be stowed.

*This work was done by Christopher J. Johnson of Johnson Space Center. Further information is contained in a TSP (see page 1).*

*This invention is owned by NASA, and a patent application has been filed. Inquiries concerning nonexclusive or exclusive license for its commercial development should be addressed to the Patent Counsel, Johnson Space Center, (281) 483-1003. Refer to MSC-24149-1.*



## Ultra-Large Solar Sail

Marshall Space Flight Center, Alabama

UltraSail is a next-generation ultra-large ( $\text{km}^2$  class) sail system. Analysis of the launch, deployment, stabilization, and control of these sails shows that high-payload-mass fractions for interplanetary and deep-space missions are possible. UltraSail combines propulsion and control systems developed for formation-flying microsattellites with a solar sail architecture to achieve controllable sail areas approaching  $1 \text{ km}^2$ . Electrically conductive CP-1 polyimide film results in sail subsystem area densities as low as  $5 \text{ g/m}^2$ . UltraSail produces thrust levels many times those of

ion thrusters used for comparable deep-space missions.

The primary innovation involves the near-elimination of sail-supporting structures by attaching each blade tip to a formation-flying microsattellite, which deploys the sail and then articulates the sail to provide attitude control, including spin stabilization and precession of the spin axis. These microsattellite tips are controlled by microthrusters for sail-film deployment and mission operations.

UltraSail also avoids the problems inherent in folded sail film, namely stressing, yielding, or perforating, by storing

the film in a roll for launch and deployment. A 5-km long by 2 micrometer thick film roll on a mandrel with a 1 m circumference (32 cm diameter) has a stored thickness of 5 cm. A 5 m-long mandrel can store a film area of  $25,000 \text{ m}^2$ , and a four-blade system has an area of  $0.1 \text{ km}^2$ .

*This work was done by Rodney Burton and Victoria Coverstone of the University of Illinois Urbana-Champaign for Marshall Space Flight Center. For more information, contact Sammy Nabors, MSFC Commercialization Assistance Lead, at [sammy.a.nabors@nasa.gov](mailto:sammy.a.nabors@nasa.gov). Refer to MFS-32524-1*

## Cooperative Three-Robot System for Traversing Steep Slopes

This system is modeled on safe human climbing of steep slopes.

NASA's Jet Propulsion Laboratory, Pasadena, California

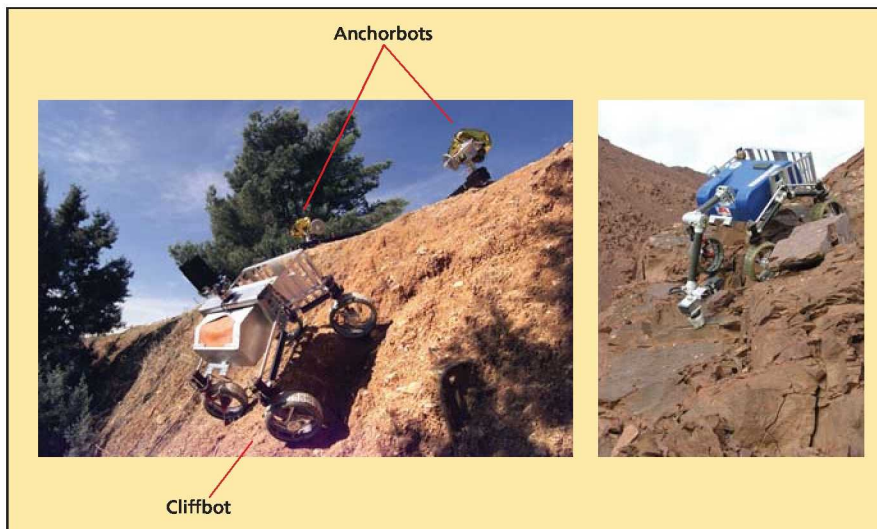
Teamed Robots for Exploration and Science in Steep Areas (TRESSA) is a system of three autonomous mobile robots that cooperate with each other to enable scientific exploration of steep terrain (slope angles up to  $90^\circ$ ). Originally intended for use in exploring steep slopes on Mars that are not accessible to lone wheeled robots (Mars Exploration

Rovers), TRESSA and systems like TRESSA could also be used on Earth for performing rescues on steep slopes and for exploring steep slopes that are too remote or too dangerous to be explored by humans.

TRESSA is modeled on safe human climbing of steep slopes, two key features of which are teamwork and safety teth-

ers. Two of the autonomous robots, denoted Anchorbots, remain at the top of a slope; the third robot, denoted the Cliffbot, traverses the slope. The Cliffbot drives over the cliff edge supported by tethers, which are payed out from the Anchorbots (see figure). The Anchorbots autonomously control the tension in the tethers to counter the gravitational force on the Cliffbot. The tethers are payed out and reeled in as needed, keeping the body of the Cliffbot oriented approximately parallel to the local terrain surface and preventing wheel slip by controlling the speed of descent or ascent, thereby enabling the Cliffbot to drive freely up, down, or across the slope.

Due to the interactive nature of the three-robot system, the robots must be very tightly coupled. To provide for this tight coupling, the TRESSA software architecture is built on a combination of (1) the multi-robot layered behavior-coordination architecture reported in "An Architecture for Controlling Multiple Robots" (NPO-30345), *NASA Tech Briefs*, Vol. 28, No. 10 (October 2004), page 65, and (2) the real-time control architecture reported in "Robot Electronics Architecture" (NPO-41784), *NASA Tech*



Left: The Cliffbot is tethered to the two Anchorbots so that it can move on the steep slope. Right: The Cliffbot performs scientific studies of the cliff.

*Briefs*, Vol. 32, No. 1 (January 2008), page 28. The combination architecture makes it possible to keep the three robots synchronized and coordinated, to use data from all three robots for decision-making at each step, and to control the physical connections among the robots. In addition, TRESSA (as in prior systems that have utilized this architecture), incorporates a capability for deterministic response to unanticipated situations from yet another architecture reported in "Control Architecture for Robotic Agent Command and Sensing" (NPO-43635), *NASA Tech Briefs*, Vol. 32, No. 10 (October 2008), page 40.

Tether tension control is a major consideration in the design and operation of TRESSA. Tension is measured by force sensors connected to each tether at the Cliffbot. The direction of the tension (both azimuth and elevation) is also measured. The tension controller combines a controller to counter gravitational force and an optional velocity

controller that anticipates the motion of the Cliffbot. The gravity controller estimates the slope angle from the inclination of the tethers. This angle and the weight of the Cliffbot determine the total tension needed to counteract the weight of the Cliffbot. The total needed tension is broken into components for each Anchorbot. The difference between this needed tension and the tension measured at the Cliffbot constitutes an error signal that is provided to the gravity controller. The velocity controller computes the tether speed needed to produce the desired motion of the Cliffbot.

Another major consideration in the design and operation of TRESSA is detection of faults. Each robot in the TRESSA system monitors its own performance and the performance of its teammates in order to detect any system faults and prevent unsafe conditions. At startup, communication links are tested and if any robot is not communicating, the system

refuses to execute any motion commands. Prior to motion, the Anchorbots attempt to set tensions in the tethers at optimal levels for counteracting the weight of the Cliffbot; if either Anchorbot fails to reach its optimal tension level within a specified time, it sends a message to the other robots and the commanded motion is not executed. If any mechanical error (e.g., stalling of a motor) is detected, the affected robot sends a message triggering stoppage of the current motion. Lastly, messages are passed among the robots at each time step (10 Hz) to share sensor information during operations. If messages from any robot cease for more than an allowable time interval, the other robots detect the communication loss and initiate stoppage.

*This work was done by Ashley Stroupe, Terrence Huntsberger, Hrand Aghazarian, Paulo Younse, and Michael Garrett of Caltech for NASA's Jet Propulsion Laboratory. Further information is contained in a TSP (see page 1). NPO-44699*

## ⚙️ Assemblies of Conformal Tanks

Space is utilized efficiently and sloshing is reduced.

*Marshall Space Flight Center, Alabama*

Assemblies of tanks having shapes that conform to each other and/or conform to other proximate objects have been investigated for use in storing fuels and oxidizers in small available spaces in upper stages of spacecraft. Such assemblies might also prove useful in aircraft, automobiles, boats, and other terrestrial vehicles in which space available for tanks is limited.

The basic concept of using conformal tanks to maximize the utilization of limited space is not new in itself: for example, conformal tanks are used in some automobiles to store windshield-washer liquid and coolant that overflows from radiators. The novelty of the present development lies in the concept of an assembly of smaller conformal tanks, as distinguished from a single larger conformal tank. In an assembly of smaller tanks, it would be possible to store different liquids in different tanks. Even if the same liquid were stored in all the tanks, the assembly would offer an advantage by reducing the mechanical disturbance caused by sloshing of fuel in a single larger tank: indeed, the requirement to reduce sloshing is critical in some applications.



This **Prototype Assembly of Conformal Tanks** was built to demonstrate the feasibility of building such an assembly to fit an approximately toroidal available volume.

The figure shows a prototype assembly of conformal tanks. Each tank was fabricated by (1) copper plating a wax tank mandrel to form a liner and (2) wrapping and curing layers of graphite/epoxy composite to form a shell supporting the liner. In this case, the conformal tank surfaces are flat

ones where they come in contact with the adjacent tanks. A band of fibers around the outside binds the tanks together tightly in the assembly, which has a quasi-toroidal shape. For proper functioning, it would be necessary to maintain equal pressure in all the tanks.

*This work was done by Tom DeLay of Marshall Space Flight Center.*

*This invention is owned by NASA, and a patent application has been filed. For further information, contact Sammy Nabors, MSFC Commercialization Assistance Lead, at sammy.a.nabors@nasa.gov. Refer to MFS-32015-1.*

## Microfluidic Pumps Containing Teflon® AF Diaphragms

**Operational temperature ranges have been extended to lower and higher limits.**

*NASA's Jet Propulsion Laboratory, Pasadena, California*

Microfluidic pumps and valves based on pneumatically actuated diaphragms made of Teflon® AF polymers are being developed for incorporation into laboratory-on-a-chip devices that must perform well over temperature ranges wider than those of prior diaphragm-based microfluidic pumps and valves. Other potential applications include implanted biomedical microfluidic devices, wherein the biocompatibility of Teflon® AF polymers would be highly advantageous. These pumps and valves have been demonstrated to function stably after cycling through temperatures from -125 to 120 °C.

These pumps and valves are intended to be successors to similar prior pumps and valves containing diaphragms made of polydimethylsiloxane (PDMS) [commonly known as silicone rubber]. The PDMS-containing valves are designed to function stably only within the temperature range from 5 to 80 °C. Undesirably, PDMS membranes are somewhat porous and retain water. PDMS is especially unsuitable for use at temperatures below 0 °C because the formation of ice crystals increases porosity and introduces microshear.

"Teflon® AF" is the trade name of family of fluoropolymers that are amorphous (in the sense of lacking crystalline structure). These polymers are less permeable and more thermally stable, relative to PDMS. These polymers are similar to other fluoropolymers in their mechanical and optical properties, in

being highly resistant to attack by many chemicals, and in retaining their desirable properties over wide temperature ranges. However, unlike other fluoropolymers, these are soluble in selected solvents; as such, they are amenable to spin coating to form membranes.

A typical microfluidic device of the type to which the present development applies includes one or more rigid glass substrate layers containing fluid-handling channels and chambers. Each pump or valve includes a polymer membrane diaphragm bonded to a glass layer or sandwiched between two glass layers, with one or more circular cutout(s) in each such glass layer to accommodate motion of the diaphragm and flows of fluids. The development effort thus far has included experiments to determine optimum combinations of ingredients and process conditions to form Teflon® AF membranes and incorporate them into pumps as diaphragms. It was found that structurally robust Teflon® AF 1600 membranes of acceptably high quality, about 50 µm thick, can be formed by means of a spin-coating process repeated at least five times and that adequate adhesion of the membranes to glass substrates could be ensured by coating the membrane-anchoring areas of the substrates by vapor deposition of chromium to a thickness of 50 Å. Chromium was removed from valve seats and other nearby substrate areas to which moving portions of diaphragms were required not to adhere.

Pumps fabricated according to the guidance provided by the experiments have been operated for more than 240 hours without delamination of membranes from substrates or any other failures. Diaphragms and valve seats of various sizes and shapes have been tested; the combination of circular diaphragms of 2 mm diameter with hemispherical valve seats was found to yield the best overall performance. Various combinations of opening and closing actuation pressures were also tested; a combination of 6 psi (41 kPa) closing pressure and -12 psi (-83 kPa) opening pressure was found to generate the highest rate of flow while preventing formation of bubbles in the pumped liquid.

Temperature-cycling tests have also been performed. The first test involved warming the pumps to 50 °C followed by cooling the pumps to -25 °C for 30 minutes. Next, the pumps were cooled to -80 °C and held there for 48 hours. Finally, the pumps were cycled from -125 to 120 °C four times over 24 hours. After each thermal cycle, pumping characteristics were measured. Interestingly, flow rates were found to be slightly increased after temperature cycling. No detrimental effects were noted after any of the temperature tests.

*This work was done by Peter Willis, Victor White, Frank Grunthaler and Mike Ikeda of Caltech and Richard A. Mathies of the University of California, Berkeley, for NASA's Jet Propulsion Laboratory. Further information is contained in a TSP (see page 1). NPO-44482*





## Transparent Conveyor of Dielectric Liquids or Particles

A high-voltage electrodynamic screen would be implemented using transparent electrodes.

John F. Kennedy Space Center, Florida

The concept of a transparent conveyor of small loose dielectric particles or small amounts of dielectric liquids has emerged as an outgrowth of an effort to develop efficient, reliable means of automated removal of dust from solar cells and from windows of optical instruments. This concept is based on the previously reported concept of an electrodynamic screen, according to which a grid-like electric field is established on and near a surface and is moved along the surface perpendicularly to the grid lines. The resulting electrodynamic forces on loose dielectric particles or dielectric liquid drops in the vicinity would move the particles or drops along the surface. In the original dust-removal application, dust particles would thus be swept out of the affected window area (see figure). Other potential applications may occur in nanotechnology — for example, involving mixing of two or more fluids and/or nanoscale particles under optical illumination and/or optical observation.

Heretofore, to implement an electrodynamic screen, one would bury a grid of parallel wires in the material below the

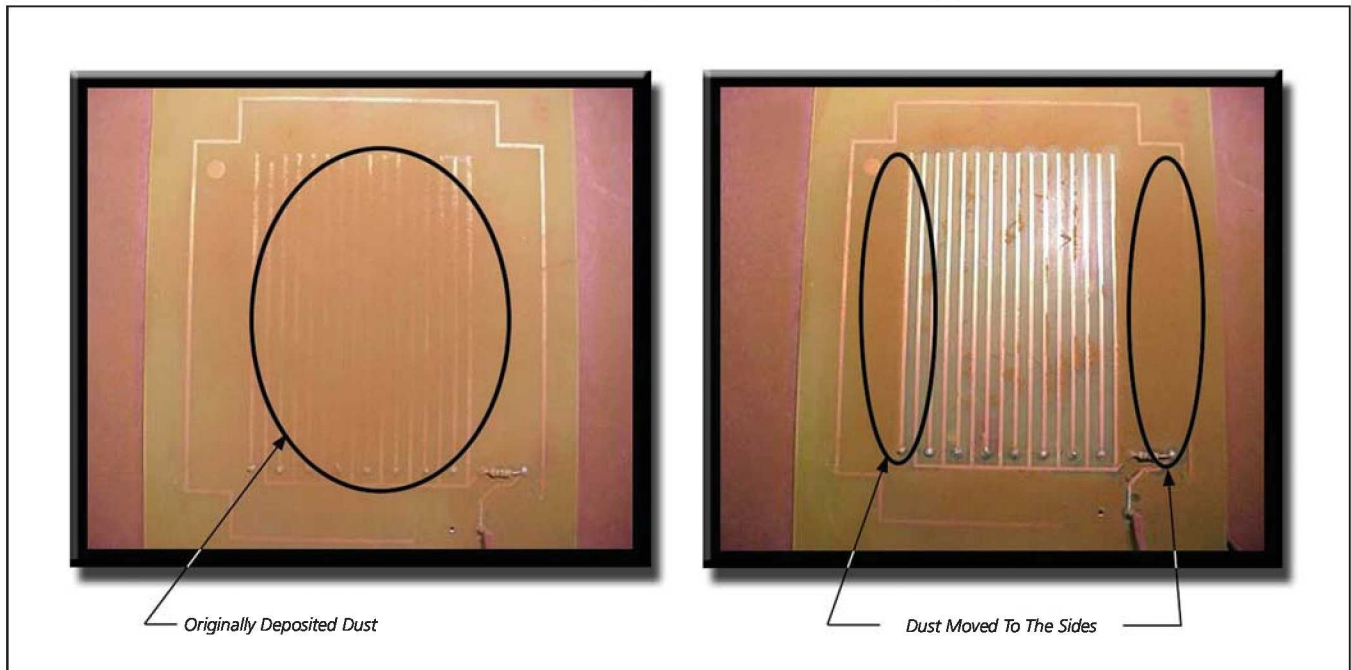
affected surface and apply suitably phased voltages to adjacent grid wires to generate the desired electric-field pattern. Because wires are opaque, this approach is not satisfactory for any application in which transparency across a defined window area is required. The present concept of a transparent conveyor is based on the same concept as that of the buried-wire implementation of an electrodynamic screen, but with a significant difference: Instead of wires, one would use electrodes made of thin layers of indium tin oxide, which are both electrically conductive and transparent.

The fabrication of such a grid of electrodes would begin with the deposition (by sputtering or thermal evaporation) of a thin, continuous layer of indium tin oxide onto a substrate along which it was desired to transport particles or liquid drops. Standard photolithographic techniques would be used to remove portions of the indium tin oxide such that the remaining portions would constitute the desired array of parallel electrodes. The

electrodes would be connected to a suitable single- or multi-phase voltage source. The exposed substrate and electrode surfaces would be coated with a layer of silicon dioxide or other transparent, electrically insulating material.

In operation in the single-phase mode, the indium tin oxide electrodes would be excited in the pattern (...AGAGA...), where A represents an applied alternating high voltage signal of amplitude  $V$  and G represents electrical ground. In a three-phase mode, the electrodes would be excited in the pattern (...ABCABC...), where A, B, and C represent the three phases of an alternating voltage of amplitude  $V$ . The frequency of alternation would determine the speed at which material would be transported. It would be necessary set  $V$  to exceed a minimum value required to initiate the transport process.

*This work was done by Carlos I. Calle of Kennedy Space Center and James G. Mantovani of Florida Institute of Technology. Further information is contained in a TSP (see page 1). KSC-12616*



A Plate Containing Embedded Electrodes was used to demonstrate the concept of an electrodynamic screen for removing dust. Dust was initially deposited in the middle of the plate, as shown at the left. After activation of the electrodynamic screen, the dust was found to have moved to the right and left sides.

# Multi-Cone Model for Estimating GPS Ionospheric Delays

This model preserves the high accuracy of the conical domain model while providing superior integrity.

NASA's Jet Propulsion Laboratory, Pasadena, California

The multi-cone model is a computational model for estimating ionospheric delays of Global Positioning System (GPS) signals. It is a direct descendant of the conical-domain model, which was described in "Conical-Domain Model for Estimating GPS Ionospheric Delays" (NPO-40930), *Software Tech Briefs*, special supplement to *NASA Tech Briefs*, September 2009, page 18. A primary motivation for the development of this model is the need to find alternatives for modeling slant delays at low latitudes, where ionospheric behavior poses an acute challenge for GPS signal-delay estimates based upon the thin-shell model of the ionosphere.

Since ionospheric signal delay contributes error to GPS position and time measurements, it is necessary to estimate the delay to correct and bound this error. Several national and international systems, denoted generally as satellite-based augmentation systems (SBASs), are under development worldwide to enhance the integrity and accuracy of GPS measurements for airline navigation.

A prominent example is the Wide Area Augmentation System (WAAS) of the United States, in which slant ionospheric delay errors and confidence bounds are derived from estimates of vertical ionospheric delay modeled on a grid at regularly spaced intervals of latitude and longitude. The estimate of vertical delay at each ionospheric grid point (IGP) is calculated from a planar fit of neighboring slant delay measurements, projected to vertical using a standard thin-shell model of the ionosphere.

Interpolation on the WAAS grid enables estimation of the vertical delay at the ionospheric pierce point (IPP) of any arbitrary user's measurement. (The IPP of a given user's measurement is the point where the ray path of the measured GPS signal intersects a reference ionospheric height.) The product of the interpolated value and the user's thin-shell obliquity factor provides an estimate of the user's ionospheric slant delay.

Two types of error restrict the accuracy of delay estimates based upon the thin-shell model: (1) error arising from the implicit assumption that, at the IPP, the electron density is independent of

the azimuthal angle, and (2) error due to an invalid obliquity factor (e.g., error due to a suboptimal choice of shell height). Under nominal conditions at mid-latitudes, the magnitude of the error incurred from these sources is small. However, at low latitudes or at mid-latitudes under disturbed conditions, the error grows due to the presence of enhanced ionization, complex ionospheric structure, and large elec-

tron-density gradients. In the conical-domain model, these sources of error are mitigated by eliminating the use of both the thin-shell model and the vertical delay grid. Instead, a user's slant delay to a given satellite is calculated directly by fitting measured slant delays for nearby ray paths to the same satellite.

The conical domain model is so named because the receiver and satellite positions define a cone with the

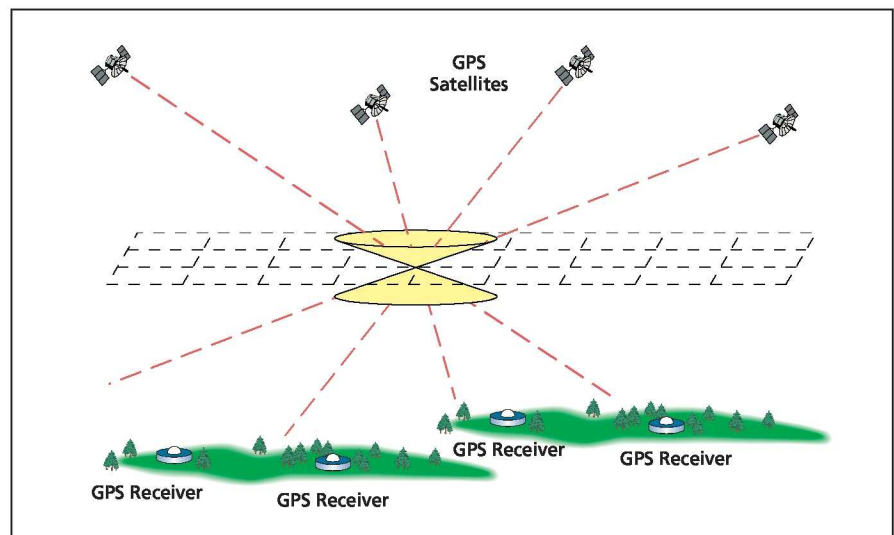


Figure 1. A Conical Domain having a vertex at a given IGP is defined, and a set of pseudo-measurements for ray paths that intersect at the IGP is fit to this conical domain.

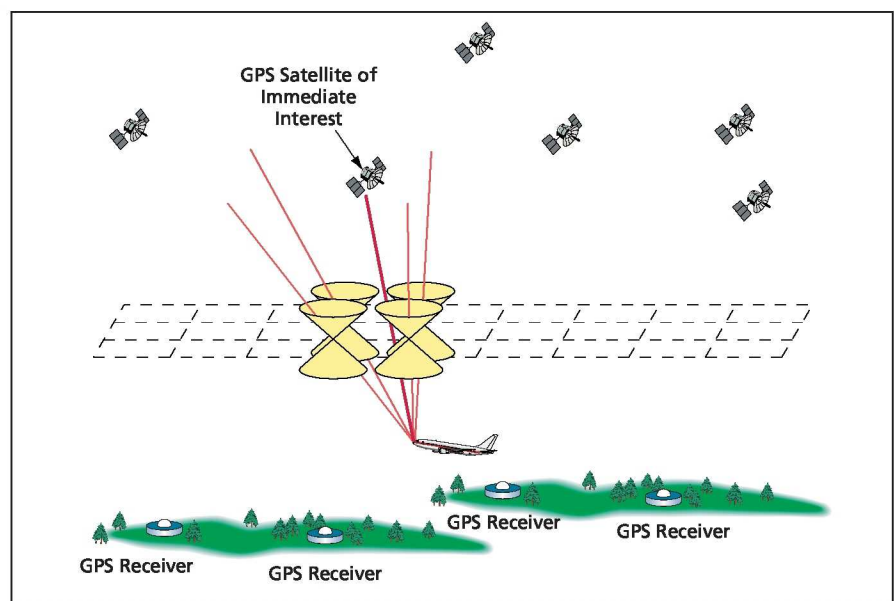


Figure 2. The Slant Delay From a Satellite of Interest to a user airplane is estimated by interpolating among slant delays for ray paths between (a) the user airplane and (b) each of the four adjacent IGPs for which pseudo-measurements have been fit to conical domains as depicted in Figure 1.

satellite position at the vertex. In an SBAS based upon the conical domain model, fits of delay on a grid of IGP are replaced with fits inside cones, each having a GPS satellite at its vertex. A user (e.g., an airplane in flight) within a given cone evaluates the delay to the satellite directly, using (1) the IPP coordinates of the line of sight to the satellite and (2) broadcast fit parameters associated with the cone.

In the context of SBAS, the conical-domain model suffers from one major limitation: each fit is comprised of relatively few measurements. Since the reliability of a fit depends upon the number of its measurements, a small number of fit measurements represent a threat to the integrity of the delay estimates based upon the fit. The multi-cone model, in which measured signals from multiple satellites are incorporated into each delay estimate, has been conceived as a means of obtaining the benefits of the conical-domain model without suffering a potentially serious loss of integrity.

The basic idea of the multi-cone model is to adapt the conical-domain model to obtain fits on an ionospheric grid. The adaptation involves multiple stages. In the first stage, the conical-domain model is used to obtain an estimate of the slant delay for each ray path

that connects a visible satellite to a specified IGP. This requires a separate fit for each satellite. Each delay estimate may be regarded as a pseudo-measurement of a signal for the satellite in question. In the second stage, the conical-domain model is turned upside down in the sense that instead of creating a cone of measurements having a satellite at its vertex and multiple receivers at its base, one forms a cone having a single receiver at the vertex and performs a fit of a set of pseudo-measurements within this cone (see Figure 1).

This process is repeated until fit parameters have been determined for cones at each IGP in a grid. It is then possible to evaluate the slant delay for any ray path that passes through both a user's position and an IGP. To evaluate the slant delay to a satellite of immediate interest from any arbitrary user position, the user first locates the IPP of the signal from that satellite and then identifies the four IGP's at the corners of the grid cell that contains this IPP. The estimates of the slant delays for the ray paths through each of these four IGP's can then be interpolated to obtain the slant delay between the user's position and the satellite of immediate interest (see Figure 2).

This estimate formally converges to the correct value in the limit as the den-

sities of participating GPS receivers and GPS satellites become very large and, simultaneously, grid cells become more nearly infinitesimal. It should be noted that the user's slant delay estimate contains information from all the signals that have been used to define the cones at the four interpolation IGP's (in contrast to fitting only data from signals emitted by the satellite of immediate interest as in the original conical-domain approach). The use of additional information in evaluating each fit serves to improve the integrity of the delay estimate while preserving the accuracy of the conical domain model.

*This work was done by Lawrence Sparks, Attila Komjathy, and Anthony Mannucci of Caltech for NASA's Jet Propulsion Laboratory.*

*In accordance with Public Law 96-517, the contractor has elected to retain title to this invention. Inquiries concerning rights for its commercial use should be addressed to:*

*Innovative Technology Assets Management  
JPL*

*Mail Stop 202-233  
4800 Oak Grove Drive  
Pasadena, CA 91109-8099  
(818) 354-2240*

*E-mail: [iaoffice@jpl.nasa.gov](mailto:iaoffice@jpl.nasa.gov)*

*Refer to NPO-40931, volume and number of this NASA Tech Briefs issue, and the page number.*

## High-Sensitivity GaN Microchemical Sensors

**This innovation enables remote detection of chemical/biological toxins in the air.**

*NASA's Jet Propulsion Laboratory, Pasadena, California*

Systematic studies have been performed on the sensitivity of GaN HEMT (high electron mobility transistor) sensors using various gate electrode designs and operational parameters. The results here show that a higher sensitivity can be achieved with a larger  $W/L$  ratio ( $W$  = gate width,  $L$  = gate length) at a given  $D$  ( $D$  = source-drain distance), and multi-finger gate electrodes offer a higher sensitivity than a one-finger gate electrode. In terms of operating conditions, sensor sensitivity is strongly dependent on transconductance of the sensor. The highest sensitivity can be achieved at the gate voltage where the slope of the transconductance curve is the largest.

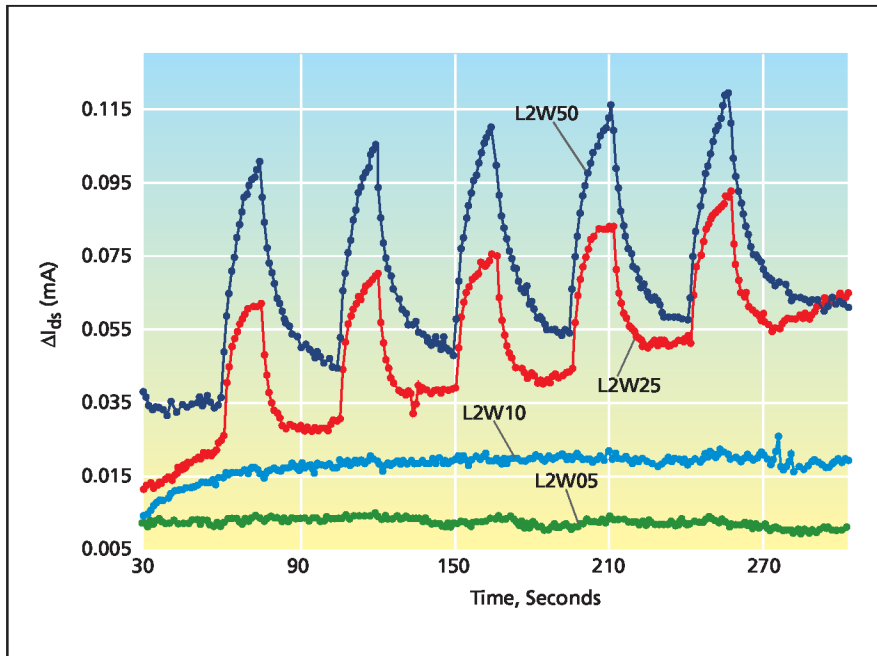
While GaN-based microchemical sensors have shown very promising performance characteristics, there has not been much understanding on how sen-

sor sensitivity can be engineered or improved. This work provides critical information about how the gate electrode of a GaN HEMT, which has been identified as the most sensitive among GaN microsensors, needs to be designed, and what operation parameters should be used for high sensitivity detection.

The figure shows  $I_{ds}$  (source-drain current) response to  $SF_6$  exposures measured using the GaN HEMT sensors fabricated with  $W = 5, 10, 25,$  and  $50 \mu m$  at  $L = 2 \mu m$ . The sensors clearly demonstrate a higher sensitivity with an increasing gate width.  $I_{ds}$  response measured using GaN HEMT sensors fabricated with  $L = 2, 4,$  and  $8 \mu m$  at  $W = 50 \mu m$  and with  $L = 2 \mu m$  at  $W = 25 \mu m$ ; (in these sensors the source-drain distance is  $DS = L + 4 \mu m$ ) show decreasing sensitivity with an increasing gate length.

Comparison between L4W50, L8W50 and L2W25 sensors, which correspond to DS8W50, DS12W50, and DS6W50 respectively, indicates that the sensor sensitivity is not simply proportional to  $I_{ds}$  or  $W/L$  (or  $W/DS$ ). The higher sensitivity achieved with the L2W25 sensor compared to the L4W50 sensor indicates that the shorter gate length plays a significant role. The results shown here suggest that sensor sensitivity is not simply proportional to the size of the gate electrode or the amount of  $I_{ds}$  of the sensor, and that a short gate length and a source-drain distance are important factors in determining the sensitivity of the sensor.

The robust, high-sensitivity GaN HEMT chemical sensors can be applied to NASA missions including *in-situ* detection of signatures of extraterrestrial life and *in-situ* planetary atmosphere



$I_{ds}$  Source-Drain Current Response to  $\text{SF}_6$  Exposures was measured using the GaN HEMT sensors fabricated with  $W = 5, 10, 25,$  and  $50 \mu\text{m}$  at  $L = 2 \mu\text{m}$ . The sensors clearly demonstrate a higher sensitivity with an increasing gate width.

analysis during planetary exploration. The sensors can be also used for health and habitat environmental monitoring for astronauts during manned missions. Due to the high thermal and chemical stability and excellent radiation hardness, GaN HEMT sensors can operate in all planetary conditions, which has not been possible for the conventional Si-based sensors. This innovation can offer a key capability for future NASA missions in extreme environments including Venus surface missions and Europa and Titan flagship missions. These micro GaN chemical sensors will be beneficial for Mars astrobiology field labs, comet nucleus sample returns, Titan in-situ, Europa surface and subsurface, and giant planet deep probe missions.

*This work was done by Kyung-ah Son, Baohua Yang, and Anna Liao of Caltech; Jeongsun Moon of HRL Laboratories, LLC; and Nicholas Prokopuk of the Naval Air Warfare Center for NASA's Jet Propulsion Laboratory. For more information, contact iaoffice@jpl.nasa.gov. NPO-45973*

## On the Divergence of the Velocity Vector in Real-Gas Flow

NASA's Jet Propulsion Laboratory, Pasadena, California

A theoretical study was performed addressing the degree of applicability or inapplicability, to a real gas, of the occasionally stated belief that for an ideal gas, incompressibility is synonymous with a zero or very low Mach number. The measure of compressibility used in this study is the magnitude of the divergence of the flow velocity vector [ $\nabla \cdot \mathbf{u}$  (where  $\mathbf{u}$  is the flow velocity)]. The study involves a mathematical derivation that begins with the

governing equations of flow and involves consideration of equations of state, thermodynamics, and fluxes of heat, mass, and the affected molecular species. The derivation leads to an equation for the volume integral of  $(\nabla \cdot \mathbf{u})^2$  that indicates contributions of several thermodynamic, hydrodynamic, and species-flux effects to compressibility and reveals differences between real and ideal gases. An analysis of the equation leads to the conclusion

that for a real gas, incompressibility is not synonymous with zero or very small Mach number. Therefore, it is further concluded, the contributions to compressibility revealed by the derived equation should be taken into account in simulations of real-gas flows.

*This work was done by Josette Bellan of Caltech for NASA's Jet Propulsion Laboratory. For more information, contact iaoffice@jpl.nasa.gov. NPO-46113*

## Progress Toward a Compact, Highly Stable Ion Clock

NASA's Jet Propulsion Laboratory, Pasadena, California

There was an update on the subject of two previous NASA Tech Briefs articles: "Compact, Highly Stable Ion Clock" (NPO-43075), Vol. 32, No. 5 (May 2008), page 63; and "Neon as a Buffer Gas for a Mercury-Ion Clock" (NPO-42919), Vol. 32, No. 7 (July 2008), page 62. To recapitulate: A developmental miniature mercury-ion clock has stability comparable to that of a hydrogen-maser clock. The ion-handling components are housed in a sealed vacuum tube,

wherein a getter pump maintains the partial vacuum, and the evacuated tube is backfilled with mercury vapor in a neon buffer gas.

There was progress in the development of the clock, with emphasis on the design, fabrication, pump-down, and bake-out of the vacuum tube (based on established practice in the traveling-wave-tube-amplifier industry) and the ability of the tube to retain a vacuum after a year of operation. Other develop-

ments include some aspects of the operation of mercury-vapor source (a small appendage oven containing HgO) so as to maintain the optimum low concentration of mercury vapor, and further efforts to miniaturize the vacuum and optical subsystems to fit within a volume of 2 L.

*This work was done by John Prestage and Sang Chung of Caltech for NASA's Jet Propulsion Laboratory. For more information, contact iaoffice@jpl.nasa.gov. NPO-44139*

## Instruments for Imaging From Far to Near

These instruments could also perform some spectral imaging functions at close range.

NASA's Jet Propulsion Laboratory, Pasadena, California

The acronym "CHAMP" (signifying "camera, hand lens, and microscope") denotes any of several proposed optoelectronic instruments that would be capable of color imaging at working distances that could be varied continuously through a range from infinity down to several millimeters. As in any optical instrument, the magnification, depth of field, and spatial resolution would vary with the working distance. For example, in one CHAMP version, at a working distance of 2.5 m, the instrument would function as an electronic camera with a magnification of 1/100, whereas at a working distance of 7 mm, the instrument would function as a microscope/electronic camera with a magnification of 4.4. Moreover, as described below, when operating at or near the shortest-working-distance/highest-magnification combination, a CHAMP could be made to perform one or more spectral imaging functions.

CHAMPs were originally intended to be used in robotic geological exploration of the Moon and Mars. The CHAMP concept also has potential for diverse terrestrial applications that could include remotely controlled or robotic geological exploration, prospecting, field microbiology, environmental surveying, and assembly-line inspection.

A CHAMP (see figure) would include two lens cells: (1) a distal cell corresponding to the objective lens assembly of a conventional telescope or microscope and (2) a proximal cell that would contain the

focusing camera lens assembly and the camera electronic image-detector chip, which would be of the active-pixel-sensor (APS) type. The distal lens cell would face outward from a housing, while the proximal lens cell would lie in a clean environment inside the housing. The proximal lens cell would contain a beam splitter that would enable simultaneous use of the imaging optics (that is, proximal and distal lens assemblies) for imaging and illumination of the field of view. The APS chip would be mounted on a focal plane on a side face of the beam splitter, while light for illuminating the field of view would enter the imaging optics via the end face of the beam splitter.

The proximal lens cell would be mounted on a sled that could be translated along the optical axis for focus adjustment. The position of the CHAMP would initially be chosen at the desired working distance of the distal lens from (corresponding to an approximate desired magnification of) an object to be examined. During subsequent operation, the working distance would ordinarily remain fixed at the chosen value and the position of the proximal lens cell within the instrument would be adjusted for focus as needed.

A CHAMP could be equipped with one or more illumination subsystem(s), one of which could be a laser probe that could be used during microscope operation. Laser light would be delivered via an optical fiber to the focal plane on the

end face of the beam splitter. The laser light would pass through the beam splitter into the imaging optics, which would focus the laser light to a small spot (typically no wider than about 10  $\mu\text{m}$ ) on the object under examination. The output end of the optical fiber could be moved in the beam-splitter-end-face focal plane to scan the laser spot across the object in order to interrogate microscopic features anywhere in the field of view. Depending on the specific application and specific instrument design, the laser light could be used as simple illumination for ordinary imaging or as excitation for one or more of several spectroscopic techniques that could include Raman spectroscopy, micro-laser-induced breakdown spectroscopy, and ultraviolet fluorescence spectroscopy.

*This work was done by Greg Mungas, John Boynton, and Cesar Sepulveda of Caltech for NASA's Jet Propulsion Laboratory. Further information is contained in a TSP (see page 1).*

*In accordance with Public Law 96-517, the contractor has elected to retain title to this invention. Inquiries concerning rights for its commercial use should be addressed to:*

*Innovative Technology Assets Management  
JPL*

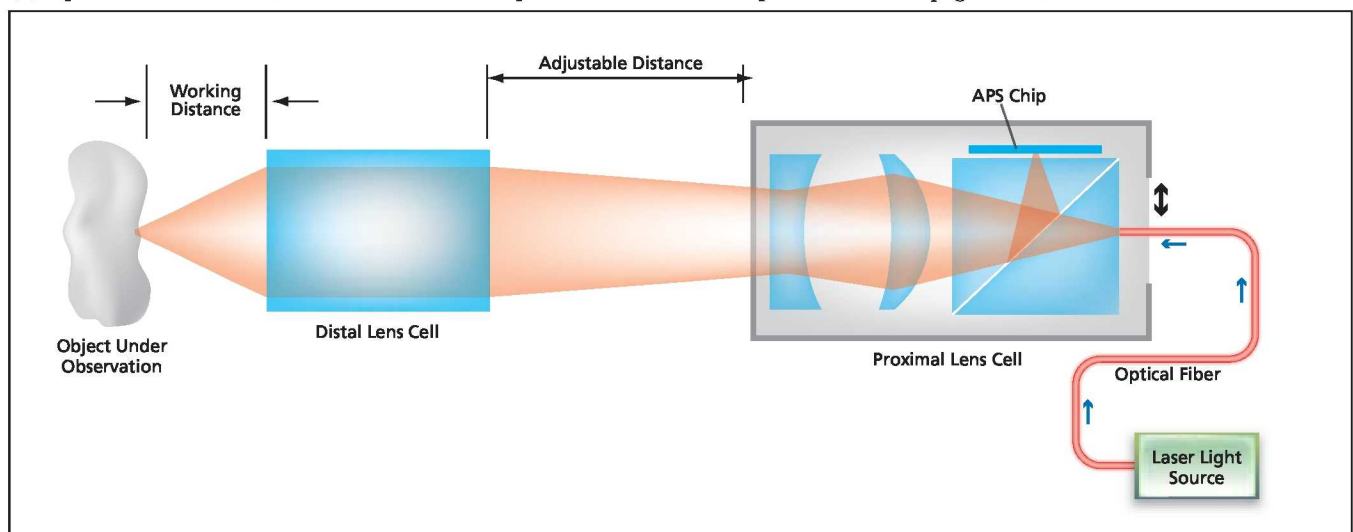
*Mail Stop 202-233*

*4800 Oak Grove Drive*

*Pasadena, CA 91109-8099*

*E-mail: iaoffice@jpl.nasa.gov*

*Refer to NPO-44780, volume and number of this NASA Tech Briefs issue, and the page number.*



The Optical Layout of a CHAMP is shown here greatly simplified and not to scale. It serves mainly to illustrate the focus adjustment and the use of the optics for both illumination and imaging.

## Reflectors Made From Membranes Stretched Between Beams

The beams could be bent to adjust reflector shapes.

NASA's Jet Propulsion Laboratory, Pasadena, California

Lightweight cylindrical reflectors of a proposed type would be made from reflective membranes stretched between pairs of identically curved and identically oriented end rails. In each such reflector, the curvature of the two beams would define the reflector shape required for the intended application. For example, the beams could be curved to define a reflector of parabolic cross section, so that light incident along the axis of symmetry perpendicular to the cylindrical axis would be focused to a line. In addition, by applying suitable forces to the ends of the beams, one could bend the beams to adjust the reflector surface figure to within a precision of the order of the wavelength of the radiation to be reflected.

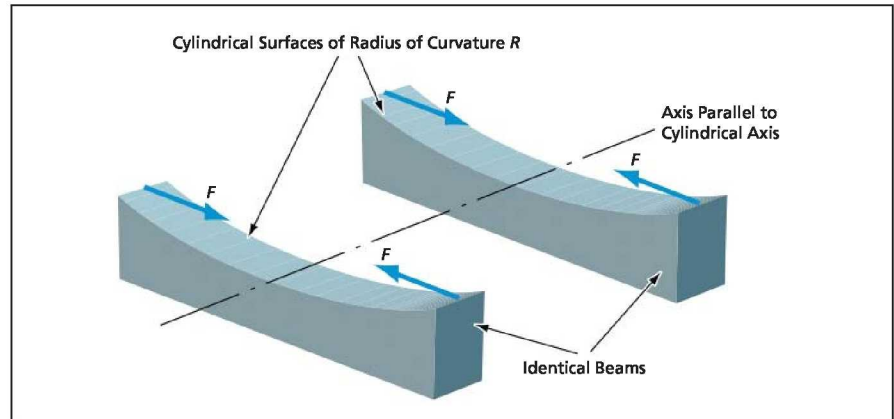
The figure depicts an example of beams shaped so that in the absence of applied forces, each would be flat on one side and would have a radius of curvature  $R$  on the opposite side. Alternatively, the curvature of the reflector-

membrane side could be other than circular. In general, the initial curvature would be chosen to optimize the final reflector shape. Then by applying forces  $F$  between the beam ends in the positions and orientations shown in the figure, one could bend beams to adjust their shape to a closer approximation of the

desired precise circular or noncircular curvature.

*This work was done by Jennifer Dooley and Mark Dragovan of Caltech and Jason Tolomeo of Lockheed-Martin for NASA's Jet Propulsion Laboratory. Further information is contained in a TSP (see page 1).*

NPO-30571



Two Identically Shaped and Oriented Beams would be bent to adjust their curvatures precisely. A reflective membrane would be stretched between the precisely curved surfaces.



## Integrated Risk and Knowledge Management Program — IRKM-P

Program helps people do work more effectively.

NASA Headquarters, Washington, DC

The NASA Exploration Systems Mission Directorate (ESMD) IRKM-P tightly couples risk management and knowledge management processes and tools to produce an effective “modern” work environment. IRKM-P objectives include: (1) to learn lessons from past and current programs (Apollo, Space Shuttle, and the International Space Station); (2) to generate and share new engineering design, operations, and management best practices through pre-existing Continuous Risk Management (CRM) procedures and knowledge-management practices; and (3) to infuse those lessons and best practices into current activities. The conceptual framework of the IRKM-P is based on the assumption that risks highlight potential knowledge gaps that might be mitigated through one or more knowledge management practices or artifacts. These same risks also serve as cues for collection of knowledge — particularly, knowledge of technical or programmatic challenges that might recur.

The main components of the IRKM-P are the following:

- **Continuous Risk Management**

The CRM process is a continuous, iterative process that identifies, analyzes, plans, tracks, controls, communicates, and documents risk through all lifecycle phases of an organization’s product developments. ESMD uses an enterprise risk management approach and a common framework for identifying, analyzing, communicating, and managing risks for ESMD and its performing organizations. Risks are communicated vertically through an escalation process — horizontal integration occurs through a multi-tiered risk management working group and board structure. This network is also used to communicate lessons learned and best practices.

- **Process 2.0**

The IRKM-P also has an important work-process-assist element called “Process 2.0,” or P20, which is modeled on the U.S. Army after-action review (AAR) process. P20s are process-focused, collegial, structured reflection events. They

rapidly deliver sustainable results through (1) focusing the team on doing work better — derived from Deming’s plan-do-check-reflect, (2) careful, discussion time management, (3) employment of structured thinking /logic techniques, and (4) enforcement of disciplined thinking to drive out actionable process improvements for the team. P20s have been used for a diverse set of team processes ranging from loads analysis to budget processes.

- **Knowledge-Based Risks**

ESMD defines Knowledge-Based Risks (KBRs) as: a risk record, with associated knowledge artifacts, that provides a story-telling narrative of how this risk was mitigated — and what worked or didn’t work. A KBR is also a means of transferring knowledge in a risk context. As key risks are mitigated, particularly risks which are likely to recur across other programs in ESMD, lessons are captured — what were the effects of mitigation activities; how were cost, schedule, and technical performance impacted, and so on. These lessons are appended to the risk record and organized in the risk tool by work breakdown structure for reuse by program and project risk managers in helping to identify new risks or develop better plans for pre-existing risks. When new candidate risks are identified, risk owners use related KBRs and other risks as inputs to developing their risk mitigation, analysis, and documentation approach. This provides a tight coupling of CRM with lessons learned. Instead of a “collect, store, and ignore” approach, KBRs form an active collection of lesson-learned, which are continually reused and updated.

- **Wiki-Enabled Teams**

Wiki-enabled teams perform a set of essential collaboration and knowledge sharing functions across the directorate. An important part of exploiting this technology has been helping teams critically examine their work processes and information architecture, which is then mapped into the tool. The wiki

provides teams an easy to use, flexible interface to collaborate on documents, conduct discussions, manage calendars, locate information, and, most importantly, work more effectively.

- **Knowledge-Sharing Forums**

Knowledge-sharing forums can range from simple lunch seminars to larger conferences, such as APPEL’s Masters Forum. A key goal in holding these forums is to provide speakers with subject matter expertise pertinent to risk drivers across ESMD. Many of these forums are recorded for later reuse.

- **Experience-Based Training**

Experience-based training involves risk management case studies, which serve as the ultimate multi-media “lessons learned” interface in our online environment. The first case developed addresses the project success story of the Space Shuttle Super Light Weight Tank development — going back to the IRKM-P framework of risks providing a cuing function, this subject was chosen because we are currently challenged by several mass-related risks — and will continue to be challenged to control mass for the heavy lift booster, lunar lander, and habitat modules. These RM cases are intended to highlight key transferrable aspects of risk management, including the identification and analysis of risks, rigorous mitigation planning, and risk trades. The proper application of risk management principles examined in these cases can help manage lifecycle costs, development schedules, and risk, resulting in safer and more reliable systems for Constellation and other future programs.

The IRKM-P continues to evolve and serves as an effective extension of management leadership to facilitate integration, collaboration, and effective work-process implementation across the complex ESMD enterprise.

*This work was done by David M. Lengyel of NASA Headquarters. Further information is contained in a TSP (see page 1). HQN-11315-1*

# LDPC Codes With Minimum Distance Proportional to Block Size

These codes offer both low decoding thresholds and low error floors.

NASA's Jet Propulsion Laboratory, Pasadena, California

Low-density parity-check (LDPC) codes characterized by minimum Hamming distances proportional to block sizes have been demonstrated. Like the codes mentioned in the immediately preceding article, the present codes are error-correcting codes suitable for use in a variety of wireless data-communication systems that include noisy channels.

The previously mentioned codes have low decoding thresholds and reasonably low error floors. However, the minimum Hamming distances of those codes do not grow linearly with code-block sizes. Codes that have this minimum-distance property exhibit very low error floors. Examples of such codes include regular LDPC codes with variable degrees of at least 3. Unfortunately, the decoding thresholds of regular LDPC codes are high. Hence, there is a need for LDPC codes characterized by both low decoding thresholds and, in order to obtain acceptably low error floors, minimum Hamming distances that are proportional to code-block sizes.

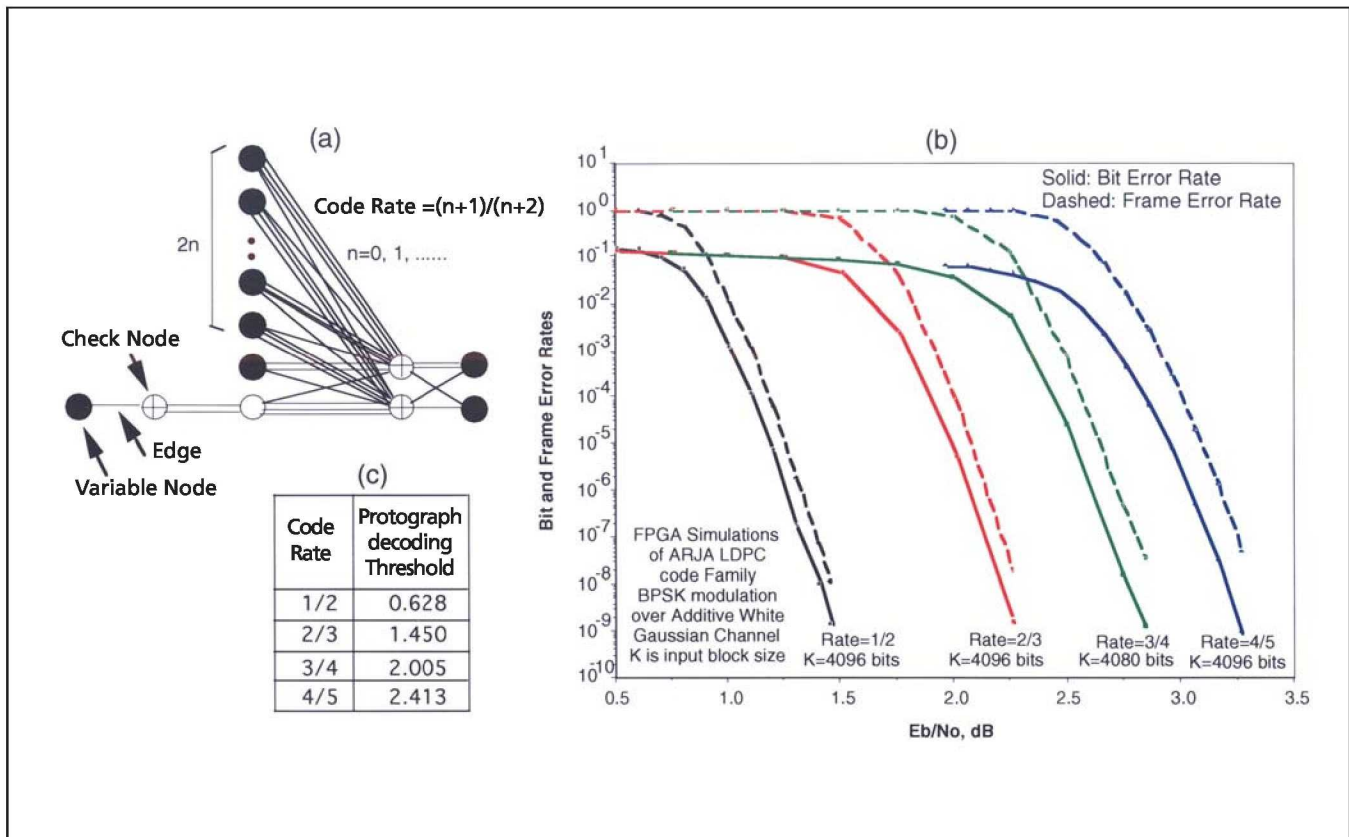
The present codes were developed to satisfy this need. The minimum Hamming distances of the present codes have been shown, through consideration of ensemble-average weight enumerators, to be proportional to code block sizes. As in the cases of irregular ensembles, the properties of these codes are sensitive to the proportion of degree-2 variable nodes. A code having too few such nodes tends to have an iterative decoding threshold that is far from the capacity threshold. A code having too many such nodes tends not to exhibit a minimum distance that is proportional to block size.

Results of computational simulations have shown that the decoding thresholds of codes of the present type are lower than those of regular LDPC codes. Included in the simulations were a few examples from a family of codes characterized by rates ranging from low to high and by thresholds that adhere closely to their respective channel capacity thresholds; the simulation results from these

examples showed that the codes in question have low error floors as well as low decoding thresholds.

As an example, the illustration shows the protograph (which represents the blueprint for overall construction) of one proposed code family for code rates greater than or equal to  $\frac{1}{2}$ . Any size LDPC code can be obtained by copying the protograph structure  $N$  times, then permuting the edges. The illustration also provides Field Programmable Gate Array (FPGA) hardware performance simulations for this code family. In addition, the illustration provides minimum signal-to-noise ratios ( $E_b/N_0$ ) in decibels (decoding thresholds) to achieve zero error rates as the code block size goes to infinity for various code rates. In comparison with the codes mentioned in the preceding article, these codes have slightly higher decoding thresholds.

The present codes offer one main disadvantage with respect to the codes described previously: These codes do not



Accumulate-Repeat-Jagged-Accumulate (ARJA) LDPC Code Family is illustrated as follows: (a) protograph, (b) performance of FPGA hardware decoder, and (c) decoding thresholds.

lend themselves to computationally efficient structures that can be implemented in high-speed encoder hardware. However, high-speed encoder implementation can be expected to be a subject of future research.

*This work was done by Dariush Divsalar, Christopher Jones, Samuel Dolinar, and Je-*

*remy Thorpe of Caltech for NASA's Jet Propulsion Laboratory.*

*In accordance with Public Law 96-517, the contractor has elected to retain title to this invention. Inquiries concerning rights for its commercial use should be addressed to:*

*Innovative Technology Assets Management  
JPL*

*Mail Stop 202-233  
4800 Oak Grove Drive  
Pasadena, CA 91109-8099  
(818) 354-2240*

*E-mail: iaoffice@jpl.nasa.gov  
Refer to NPO-42063, volume and number of this NASA Tech Briefs issue, and the page number.*

## ➤ Constructing LDPC Codes From Loop-Free Encoding Modules

High-speed iterative decoders can readily be implemented in hardware.

NASA's Jet Propulsion Laboratory, Pasadena, California

A method of constructing certain low-density parity-check (LDPC) codes by use of relatively simple loop-free coding modules has been developed. The subclasses of LDPC codes to which the method applies includes accumulate-repeat-accumulate (ARA) codes, accumulate-repeat-check-accumulate codes, and the codes described in "Accumulate-Repeat-Accumulate-Accumulate Codes" (NPO-41305), *NASA Tech Briefs*, Vol. 31, No. 9 (September 2007), page 90. All of the affected codes can be characterized as serial/parallel (hybrid) concatenations of such relatively simple modules as accumulators, repetition codes, differentiators, and punctured single-parity check codes. These are error-correcting codes suitable for use in a variety of wireless data-communication systems that include noisy channels. These codes can also be characterized as hybrid turbo-like codes that have projected graph or protograph representations (for example see figure); these characteristics make it possible to design high-speed iterative decoders that utilize belief-propagation algorithms.

The present method comprises two related submethods for constructing LDPC codes from simple loop-free modules with circulant permutations. The first submethod is an iterative encoding method based on the erasure-decoding algorithm. The computations required by this method are well organized because they involve a parity-check matrix having a block-circulant structure.

The second submethod involves the use of block-circulant generator matrices. The encoders of this method are very similar to those of recursive convolutional codes. Some encoders according to this second submethod have been implemented in a small field-programmable gate array that operates at a speed of 100 megasymbols per second.

By use of density evolution (a computational-simulation technique for analyzing performances of LDPC codes), it has been shown through some examples that as the block size goes to infinity, low iterative decoding thresholds close to channel capacity limits can be achieved for the codes of the type in question having low maximum variable node de-

grees. The decoding thresholds in these examples are lower than those of the best-known unstructured irregular LDPC codes constrained to have the same maximum node degrees. Furthermore, the present method enables the construction of codes of any desired rate with thresholds that stay uniformly close to their respective channel capacity thresholds.

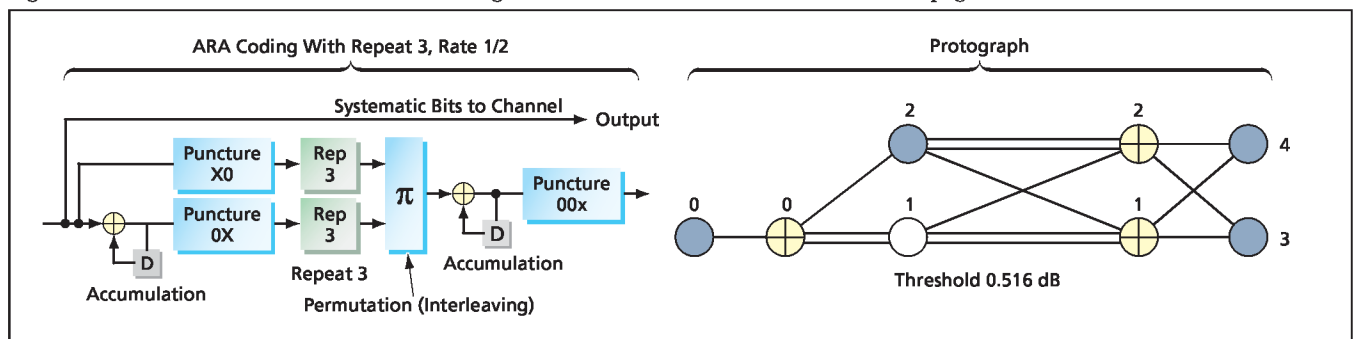
*This work was done by Dariush Divsalar, Samuel Dolinar, Christopher Jones, Jeremy Thorpe, and Kenneth Andrews of Caltech for NASA's Jet Propulsion Laboratory.*

*In accordance with Public Law 96-517, the contractor has elected to retain title to this invention. Inquiries concerning rights for its commercial use should be addressed to:*

*Innovative Technology Assets Management  
JPL*

*Mail Stop 202-233  
4800 Oak Grove Drive  
Pasadena, CA 91109-8099  
(818) 354-2240*

*E-mail: iaoffice@jpl.nasa.gov  
Refer to NPO-42042, volume and number of this NASA Tech Briefs issue, and the page number.*



A Simple Rate-1/2 ARA Code is depicted here with its protograph representation as an example of codes to which the present method applies. An encoder for this code includes a precoder in the form of a punctured accumulator.





### MMICs With Radial Probe Transitions to Waveguides

A document presents an update on the innovation reported in “Integrated Radial Probe Transition From MMIC to Waveguide” (NPO-43957), *NASA Tech Briefs* Vol. 31, No. 5 (May 2007), page 38. To recapitulate: To enable operation or testing of a monolithic microwave integrated circuit (MMIC), it is necessary to mount the MMIC in a waveguide package that typically has cross-sectional waveguide dimensions of the order of a few hundred microns. A radial probe transition between an MMIC operating at 340 GHz and a waveguide had been designed (but not yet built and tested) to be fabricated as part of a monolithic unit that would include the MMIC.

The radial probe could readily be integrated with an MMIC amplifier because the design provided for fabrication of the transition on a substrate of the same material (InP) and thickness (50  $\mu\text{m}$ ) typical of substrates of MMICs that can operate above 300 GHz. As illustrated in the updated document by drawings, photographs, and plots of test data, the concept has now been realized by designing, fabricating, and testing several MMIC/radial-probe integrated-circuit chips and designing and fabricating a waveguide package to contain each chip.

*This work was done by Lorene Samoska, Goutam Chattopadhyay, David Pukala, Mary Soria, King Man Fung, and Todd Gaier of Caltech for NASA’s Jet Propulsion Laboratory, and Vesna Radisic, Stella Makishi, William Deal, and Richard Lai of Northrop Grumman Corporation (NGC). The work was sponsored under the DARPA SWIFT program and the contributors would like to acknowledge the support of Dr. Mark Rosker (DARPA) and Dr. H. Alfred Hung (Army Research Laboratory). Further information is contained in a TSP (see page 1). NPO-45460*

### Tests of Low-Noise MMIC Amplifier Module at 290 to 340 GHz

A document presents data from tests of a low-noise amplifier module operating in the frequency range from 290 to 340 GHz — said to be the highest-frequency low-noise, solid-state amplifier ever developed. The module comprised a three-stage monolithic microwave integrated circuit (MMIC) amplifier integrated with radial probe MMIC/waveguide transitions and contained in a compact waveguide package, all according to the concepts described in the immediately preceding article and in the referenced prior article, “Integrated Radial Probe Transition From MMIC to Waveguide” (NPO-43957), *NASA Tech Briefs* Vol. 31, No. 5 (May 2007), page 38.

The tests included measurements by the Y-factor method, in which noise figures are measured repeatedly with an input noise source alternating between an “on” (hot-load) condition and an “off” (cold-load) condition. (The Y factor is defined as the ratio between the “on” and “off” noise power levels.) The test results showed that, among other things, the module exhibited a minimum noise figure of about 8.7 dB at 325 GHz and that the gain at that frequency under the bias conditions that produced the minimum noise figure was between about 9 and 10 dB.

*This work was done by Todd Gaier, Lorene Samoska, and King Man Fung of Caltech for NASA’s Jet Propulsion Laboratory, and William Deal, Xiaobing Mei, and Richard Lai of Northrop Grumman Corporation (NGC). The work was sponsored under the DARPA SWIFT program and the contributors would like to acknowledge the support of Dr. Mark Rosker (DARPA) and Dr. H. Alfred Hung (Army Research Laboratory). Further information is contained in a TSP (see page 1). NPO-45461*

### Extending Newtonian Dynamics to Include Stochastic Processes

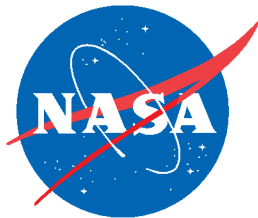
A paper presents further results of continuing research reported in several previous *NASA Tech Briefs* articles, the two most recent being “Stochastic Representations of Chaos Using Terminal Attractors” (NPO-41519), [Vol. 30, No. 5 (May 2006), page 57] and “Physical Principle for Generation of Randomness” (NPO-43822) [Vol. 33, No. 5 (May 2009), page 56]. This research focuses upon a mathematical formalism for describing postinstability motions of a dynamical system characterized by exponential divergences of trajectories leading to chaos (including turbulence as a form of chaos).

The formalism involves fictitious control forces that couple the equations of motion of the system with a Liouville equation that describes the evolution of the probability density of errors in initial conditions. These stabilizing forces create a powerful terminal attractor in probability space that corresponds to occurrence of a target trajectory with probability one. The effect in configuration space (ordinary three-dimensional space as commonly perceived) is to suppress exponential divergences of neighboring trajectories without affecting the target trajectory. As a result, the postinstability motion is represented by a set of functions describing the evolution of such statistical quantities as expectations and higher moments, and this representation is stable.

*This work was done by Michail Zak of Caltech for NASA’s Jet Propulsion Laboratory. Further information is contained in a TSP (see page 1). NPO-45594*







National Aeronautics and  
Space Administration